Cell Reports

Article

B Cell Speed and B-FDC Contacts in Germinal Centers Determine Plasma Cell Output via Swiprosin-1/EFhd2

Graphical Abstract

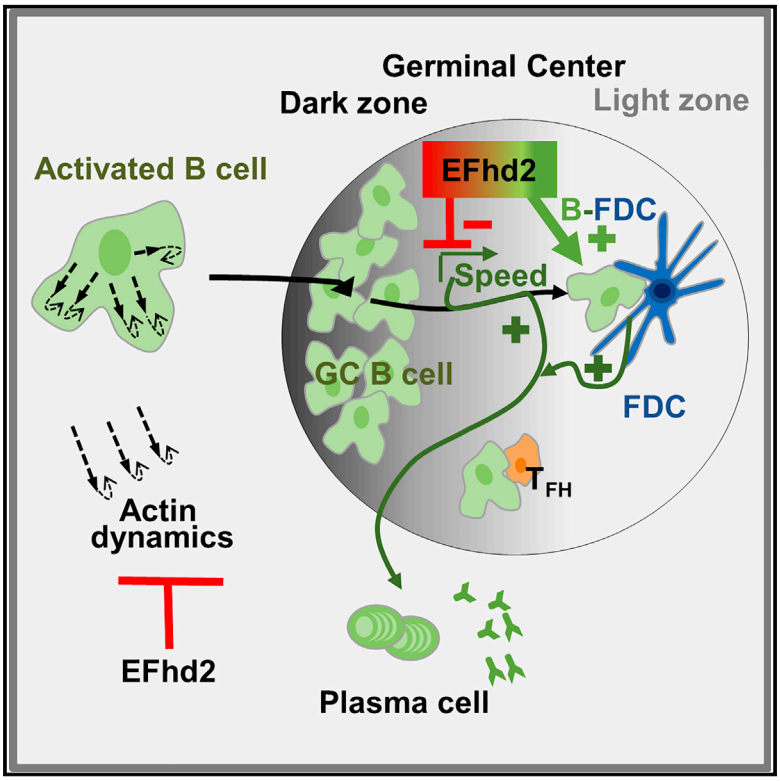

Highlights

- EFhd2 limits migration of GC B cells and hapten-specific immunity
- Fast GC B cells are selected earlier and prone to differentiate
- EFhd2 fosters contacts of GC B cells with follicular dendritic cells
- Contact of fast GC B cells with follicular dendritic cells is decisive

Authors

Dorothea Reimer, Michael Meyer-Hermann, Asylkhan Rakhymzhan, ..., Anja E. Hauser, Raluca A. Niesner, Dirk Mielenz

Correspondence

dirk.mielenz@fau.de

In Brief

Reimer et al. show that EFhd2 restricts migration of germinal center B cells and hapten-specific immunity. Selection of speedy germinal center B cells occurs earlier and they are more likely to differentiate. EFhd2 supports contact of germinal center B cells with follicular dendritic cells, enabling successful competition of rapidly migrating germinal center B cells.

Reimer et al., 2020, Cell Reports *32*, 108030
August 11, 2020
https://doi.org/10.1016/j.celrep.2020.108030

CellPress

Cell Reports

CellPress
OPEN ACCESS

Article

B Cell Speed and B-FDC Contacts in Germinal Centers Determine Plasma Cell Output via Swiprosin-1/EFhd2

Dorothea Reimer,[1] Michael Meyer-Hermann,[2] Asylkhan Rakhymzhan,[3] Tobit Steinmetz,[1] Philipp Tripal,[4] Jana Thomas,[1] Martin Boettcher,[5] Dimitrios Mougiakakos,[5] Sebastian R. Schulz,[1] Sophia Urbanczyk,[1] Anja E. Hauser,[3,6] Raluca A. Niesner,[3,7,8] and Dirk Mielenz[1,8,9,*]

[1]Division of Molecular Immunology, Universitätsklinikum Erlangen, Nikolaus-Fiebiger-Zentrum, FAU Erlangen-Nürnberg, Erlangen, Germany
[2]Department of Systems Immunology and Braunschweig, Integrated Centre of Systems Biology, Helmholtz Center for Infection Research, Braunschweig, Germany
[3]Deutsches Rheumaforschungszentrum (DRFZ), Berlin, Germany
[4]Optical Imaging Center (OICE), Universitätsklinikum Erlangen, FAU Erlangen-Nürnberg, Erlangen, Germany
[5]Department of Internal Medicine V, Universitätsklinikum Erlangen, FAU Erlangen-Nürnberg, Erlangen, Germany
[6]Charité – University Medicine, Berlin, Germany
[7]Dynamic and Functional In Vivo Imaging, Veterinary Medicine, Freie Universität, Berlin, Germany
[8]These authors contributed equally
[9]Lead Contact
*Correspondence: dirk.mielenz@fau.de
https://doi.org/10.1016/j.celrep.2020.108030

SUMMARY

Plasma cells secreting affinity-matured antibodies develop in germinal centers (GCs), where B cells migrate persistently and directionally over defined periods of time. How modes of GC B cell migration influence plasma cell development remained unclear. Through genetic deletion of the F-actin bundling protein Swiprosin-1/EF-hand domain family member 2 (EFhd2) and by two-photon microscopy, we show that EFhd2 restrains B cell speed in GCs and hapten-specific plasma cell output. Modeling the GC reaction reveals that increasing GC B cell speed promotes plasma cell generation. Lack of EFhd2 also reduces contacts of GC B cells with follicular dendritic cells *in vivo*. Computational modeling uncovers that both GC output and antibody affinity depend quantitatively on contacts of GC B cells with follicular dendritic cells when B cells migrate more persistently. Collectively, our data explain how GC B cells integrate speed and persistence of cell migration with B cell receptor affinity.

INTRODUCTION

The development of memory B cells and long-lived plasma cells (PCs) secreting affinity-matured antibodies (Abs) (Berek et al., 1991) depends on the germinal center (GC) reaction. GCs are transient structures that form in secondary lymphatic organs around the follicular dendritic cell (FDC) network ~4 days after T-cell-dependent (TD) antigen challenge (Gatto and Brink, 2010). Mature GCs are highly ordered structures consisting of histologically distinct regions, the dark zone (DZ) and the light zone (LZ), the latter of which is centered on chemokine (C-X-C motif) ligand 13 (Cxcl13)-expressing FDCs (Victora and Nussenzweig, 2012). Typically, GCs formed in response to alum precipitated haptenated model antigens last ~21–28 days and then resolve as antigen becomes limiting and Ab feedback ensues (Gatto and Brink, 2010). Long-lasting or even chronic GCs develop after immunization with particulate antigen, such as sheep red blood cells (SRBCs) (Dogan et al., 2009), in response to certain infections as a consequence of hyperimmunization or naturally in the Peyer's patches. Immunoglobulin (Ig) gene pedigrees derived from GC B cells (Berek et al., 1991) suggested a Darwinian mechanism of Ab affinity maturation. These observed Ig gene mutation rates are reconciled with DZ/LZ architecture of GCs and cell-cycle duration in the cyclic-reentry model of the GC reaction (Kepler and Perelson, 1993). Accordingly, somatic hypermutation (SHM) occurs in the DZ and clonal selection occurs in the LZ, predicting a requirement for interzonal B cell migration. *In vivo* multiphoton microscopy corroborated this prediction, with C-X-C motif chemokine receptor 4 (Cxcr4)-expressing centroblasts migrating from the DZ to the LZ and Cxcr5-expressing centrocytes migrating from the LZ to the DZ (Hauser et al., 2007). GC B cells migrate in a directed manner (O'Connor et al., 2011), whereby the net flow appears to be from the DZ to the LZ (Beltman et al., 2011), with only few B cells migrating back into the DZ (Victora et al., 2010). Tagging GC B cells with photoactivatable GFP *in vivo* has revealed that those B cells with superior antigen presentation ability are preferentially selected by T follicular helper (Tfh) cells, resulting in their migration back into the DZ and increased PC generation (Victora et al., 2010). There is evidence that B cell/T

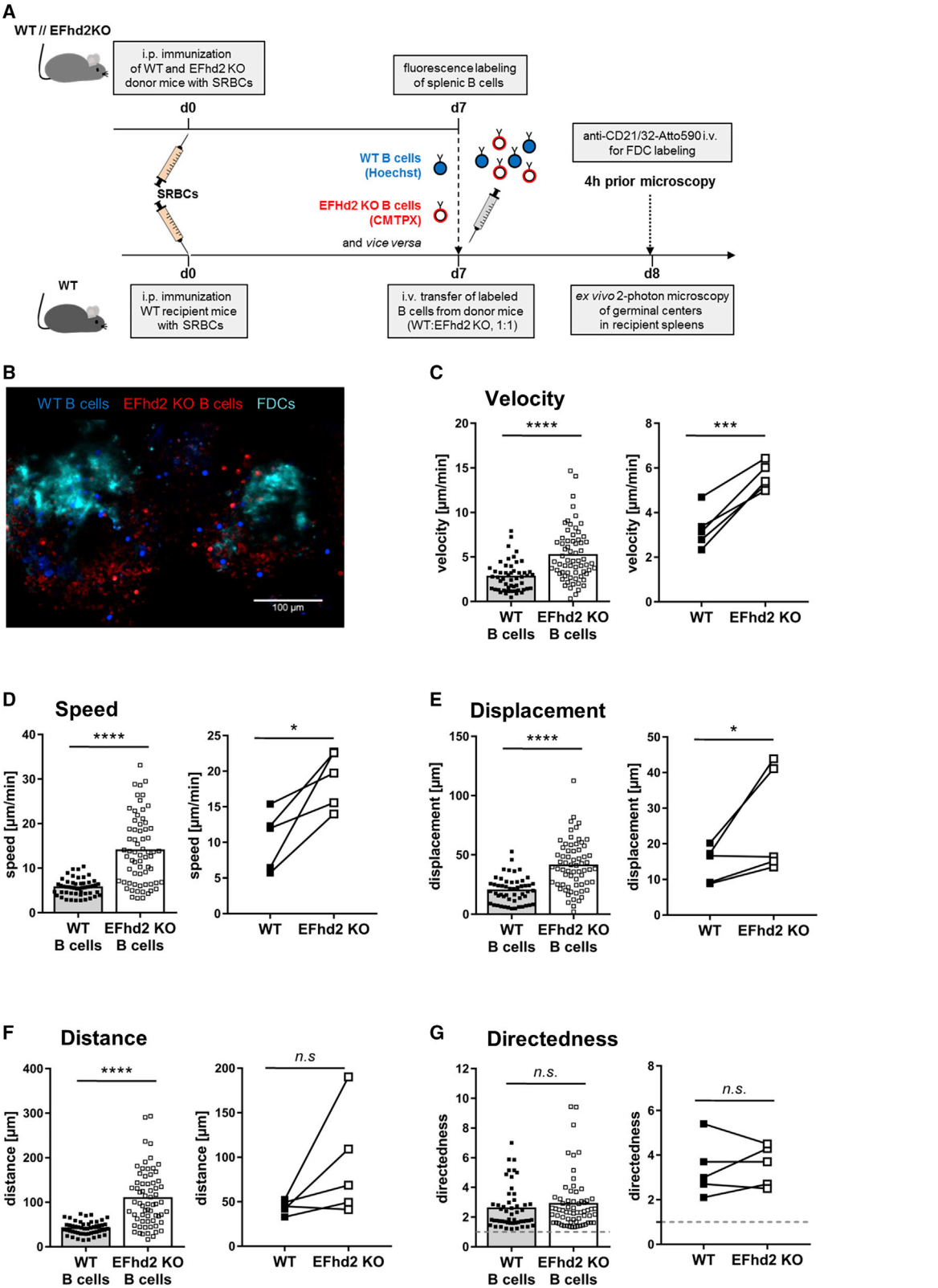

(legend on next page)

cell interactions determine the number of divisions of a B cell in the DZ (Meyer-Hermann et al., 2012). B cell clones carrying selected B cell receptor (BCR) with comparably high affinity are predominantly found in the PC compartment, while memory B cells harbor less affine BCR genes and arise earlier in the GC reaction (Weisel et al., 2016). As PCs carry Ig genes encoding higher affine BCRs and later Abs, a role for BCR signaling in addition to BCR-mediated endocytosis in dictating GC fate toward the PC program is not too speculative. Indeed, initiation of the PC program requires BCR contact with antigen contained in immune complexes bound on FDCs, followed by completion of the PC program by signals derived from Tfh cells (Kräutler et al., 2017) and specialized stromal cells localized at the T cell/B cell border (Zhang et al., 2018b). In line, B cells directly test BCR affinity on antigen presented by FDCs through force application via myosin II motors in a specialized GC synapse (Natkanski et al., 2013; Nowosad et al., 2016). Only BCR signaling, together with CD40 stimulation, enables centrocytes to upregulate Myc (Luo et al., 2018), highlighting a role for BCR signaling and T cell help in the selection of GC cells. Whereas transcription factors such as Irf4 (Klein et al., 2006), Myc (Calado et al., 2012), or Rel (Heise et al., 2014) that direct the cell fate in GCs have been well characterized, proteins linking the BCR or CD40 to GC output are less established. Those proteins might be found among those controlling B cell migration or B cell/FDC interaction in GCs (Tolar, 2017), because a main task of B cells having undergone and survived SHM in the DZ (Mayer et al., 2017) is to find antigen bound on FDCs as well as a cognate Tfh cell. In line, many reports emphasize the importance of cell migration patterns for GC dynamics, particularly for their PC output (reviewed in Victora and Nussenzweig, 2012). However, it remains elusive how different cell migration patterns directly impact the GC reaction and, consequently, PC maturation and which molecules within B cells drive their motility behavior. Swiprosin-1/EF-hand domain family member 2 (EFhd2; also known as Swiprosin-1, and not to be confused with Swiprosin-2/EFhd1; Dütting et al., 2011) is a ~30-kDa Ca^{2+}- and F-actin-binding protein (Hagen et al., 2012; Huh et al., 2013; Kwon et al., 2013) with a C-terminal coiled-coil domain and functional SH3-binding sites at the N terminus (Kroczek et al., 2010). Null mutation of EFhd2 (EFhd2KO) revealed that EFhd2 negatively controls GC expansion in response to secondary *Nippostrongylus brasiliensis* infection (Brachs et al., 2014). EFhd2 also controls development of IgG1 and IgE PCs as well as IgM and IgE serum Abs in response to infection with *N. brasiliensis* (Brachs et al., 2014) in a B-cell-intrinsic manner. How EFhd2 controls GC-derived PC generation and whether EFhd2 controls Ab quality was unknown. EFhd2 supports lamellipodia formation, lung cancer, and melanoma metastasis as well as macrophage migration through regulation of actin dynamics by Rho GTPases (Fan et al., 2017; Huh et al., 2015; Tu et al., 2018; Zhang et al., 2018a). Based thereupon, we hypothesized that EFhd2 controls the GC reaction and PC development via control of actin dynamics and cell migration. Hence, we analyzed B cell dynamics of EFhd2 wild-type (WT) and knockout (KO) B cells *in vitro* and *in vivo* using two-photon microscopy, together with *in silico* modeling and a detailed kinetic analysis of the GC and PC response against nitrophenol (NP)-keyhole limpet hemocyanin (KLH). We found that EFhd2 limits B cell migration and that enhanced B cell migration through lack of EFhd2 leads to increased PC output. However, a mathematically predicted increase in BCR affinity was counterbalanced by reduced interactions of EFhd2KO B cells with FDCs. Using this iterative approach, we defined the general concept (independently of EFhd2KO) that cell migration alone cannot elicit stronger GC reactions or Ab affinity, and B cell/FDC interactions are required to support the accelerating effect of B cell migration.

RESULTS

EFhd2KO B Cells Migrate Faster in Germinal Centers

To test whether EFhd2 affects B cell migration and PC generation, we isolated and labeled EFhd2WT and EFhd2KO B cells (Brachs et al., 2014) from SRBC-immunized mice and transferred them back into SRBC-immunized WT recipients (Figure 1A). Migration of fluorescently labeled B cells in GCs and through the FDC network was assessed in living spleen by multiphoton microscopy (Heinig et al., 2014; Rakhymzhan et al., 2017) (Video S1; Figure 1B). Hereby, we assessed several parameters: (1) velocity, (2) speed, (3) distance, (4) displacement, and (5) directedness (Figure 1C–1G; see Figure S1 for definitions and explanations). EFhd2KO B cells migrated approximately two times faster in GCs in competition with WT B cells, with both mean velocity and speed being elevated (Figure 1C, D). Displacement of EFhd2KO B cells and covered distance were proportionally enhanced (Figure 1E, F), revealing unaltered directedness (displacement/distance; Masuzzo et al., 2016) (Figure 1G), although EFhd2 has been proposed to determine the

Figure 1. EFhd2 Deficiency Enhances B Cell Motility in GCs

(A) WT and EFhd2KO donor as well as WT recipient mice were immunized intraperitoneally (i.p.) with SRBCs. At day 7, splenic B cells from donor mice were isolated and fluorescently labeled. WT B cells, Hoechst, EFhd2KO B cells, CMTPX, and vice versa, mixed in a 1:1 ratio, were transferred intravenously (i.v.) into WT recipient mice. One day after transfer, the FDC network was labeled via i.v. application of anti-CD21/32-Atto590 Fab_2-Ab, and migration of WT and EFhd2KO B cells within splenic GC was tracked.

(B) Representative image of two adjacent GCs, identified via the FDC networks (turquoise, anti-CD21/32-Atto590), containing WT B cells (blue, Hoechst) and EFhd2KO B cells (red, CMTPX). Scale bar, 100 μm.

(C–G) Plots on the left side display WT and EFhd2KO B cells tracked within one representative recipient mouse (one dot = one cell). Plots on the right side show mean values for WT and EFhd2KO B cells in five independent recipient mice (one dot = one mouse).

(C and D) Analysis of cell movement by cell velocity (C) and speed (D).

(E and F) Analysis of the actually covered paths quantified by displacement (E) and distance (F).

(G) The directedness of cell migration was calculated as the ratio of distance to displacement.

Data are represented as mean values; statistics: N = 2, n = 5; significance was analyzed using Mann-Whitney test for single cell comparison (****$p < 0.0001$, left panels in C–G) and paired t test for comparing mean values of recipient mice (nonsignificant [*n.s.*], $p > 0.05$; *$p \leq 0.05$; ***$p \leq 0.001$, right panels in C–G).

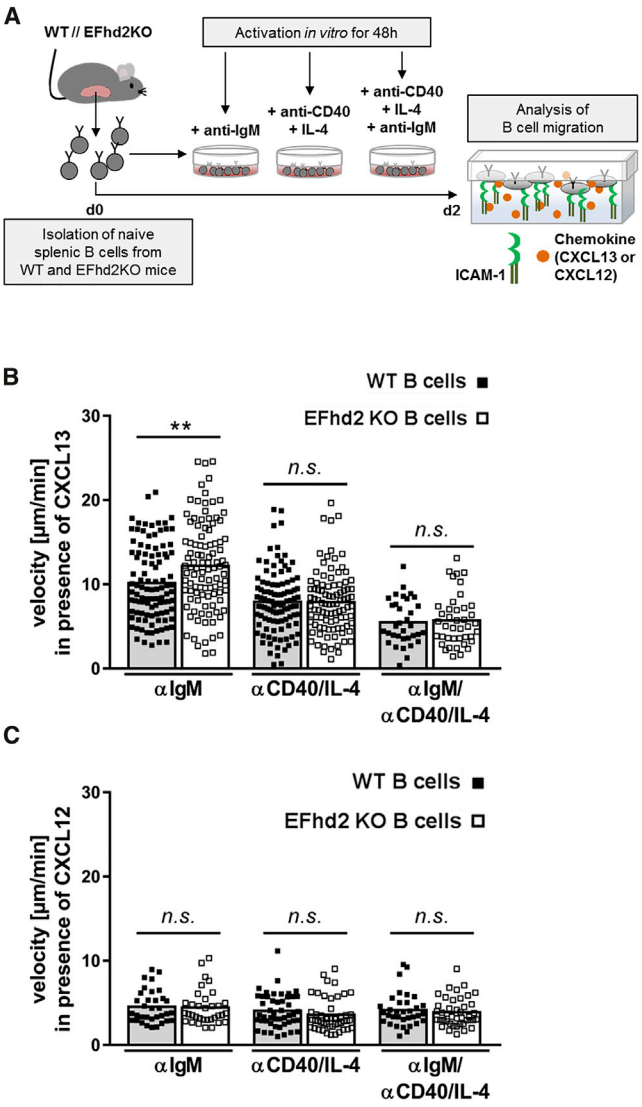

Figure 2. BCR Activation Enhances Migration of EFhd2KO B Cells on ICAM-1 and CXCL13

(A) Naive splenic B cells from WT and EFhd2KO mice were isolated and activated with anti-IgM Ab, anti-CD40 Ab + IL-4, or anti-IgM Ab + anti-CD40 Ab + IL-4 for 48 h.

(B and C) B cell migration on ICAM-1 in the presence of CXCL13 (B) or CXCL12 (C) was analyzed by spinning disc confocal microscopy. Datasets are shown for individual cells (one dot = one B cell) activated as described above. Statistics: N = 2, n = 2–3; significance was analyzed using Mann-Whitney test (*n.s.* > 0.05; **p ≤ 0.01).

direction of cell protrusions (Huh et al., 2015). Importantly, the speed of WT B cells was exactly as reported previously (Allen et al., 2007; Hauser et al., 2007; Schwickert et al., 2007). Migration, activation, and attachment of B cells is dictated by regulated expression of chemokine receptors Cxcr4 and Cxcr5, integrins, and their ligands, such as the lymphocyte-function-associated antigen 1 (LFA-1)/intercellular adhesion molecule 1 (ICAM-1) combination, as well as by B cell activation (Carrasco et al., 2004; Liu et al., 2016; reviewed in Victora and Nussenzweig, 2012). The faster migration of EFhd2KO B cells *in vivo* was not due to altered expression of Cxcr4, Cxcr5, LFA-1, very late antigen 4 (VLA-4), ICAM-1, or ICAM-2 (Figure S2). We next wished to determine which activating stimulus triggers EFhd2KO B cells. Since GC B cells have received a plethora of signals that cannot be dissected, we measured chemokinesis of SiR-actin-labeled B cells on recombinant ICAM-1Fc fusion protein (Liu et al., 2016) (Videos S2 and S3; Figure 2A). Anti-BCR-activated, but not anti-CD40/interleukin-4 (IL-4)-activated, EFhd2KO B cells migrated faster on ICAM-1 *in vitro* in response to Cxcl13 (triggering Cxcr5) (Figure 2B), but not to Cxcl12 (triggering Cxcr4) (Figure 2C). Intriguingly, BCR activation in combination with anti-CD40/IL-4 stimulation arrested B cell migration (Figure 2B) in both WT and EFhd2KO B cells. Taken together, EFhd2 limits B cell migration in GCs and *in vitro*. In particular, BCR activation appears to modulate EFhd2-restricted B cell migration.

Computational Modeling of GC Dynamics Based on Experimentally Determined Parameters of B Cell Migration

To test whether more rapid cell migration modulates GC responses we supplied an established mathematical model of the GC reaction (Binder and Meyer-Hermann, 2016; Figge et al., 2008; Meyer-Hermann, 2014; Meyer-Hermann et al., 2009, 2012) with the B cell migration data (shown in Figure 1). As EFhd2KO B cells migrated approximately two times faster (compare Figure 1), we simulated GCs with normal B cell migration rates (7.5 μmin/min/1.5 min persistence time, black lines) and two times faster B cells (15 μmin/min/1.5 min persistence time, pink lines). Faster migration may also be the result of increased directional persistence (Maiuri et al., 2015). We therefore also modeled B cells with two times and four times more persistence (7.5 μmin/min/3.0 min persistence and 7.5 μmin/min/6.0 min persistence, green and blue lines) and with two-times-faster-migrating B cells with a 2-fold increased persistence (7.5 μmin/min/3.0 min persistence, red line). Elevating cell migration or persistence *in silico* was sufficient to elicit a dose-dependent increase in the total number of GC and output cells (PCs and memory B cells) (Figures 3A and 3B). Importantly, the effect of speed was more dominant than the effect of persistence (Figure 3B). Predicted affinity maturation of GC B cells was unaltered by speed or persistence, whereas doubled speed, but not doubled persistence, predicted a small (~15%) increase in affinity of GC output cells (Figure 3C). By plotting selection probability versus affinity, it became evident that faster B cells are likely to be selected early (days 3–5), but not later (days 5–9) (Figure 3D). Taken together, increasing cell migration and persistence in simulated GCs led to the following expectations that were evaluated in our model system, EFhd2KO mice (experimentators were blinded to the results of the simulation): (1) increased GC B cell numbers, (2) enhanced PC output, and (3) a moderate increment of the mean affinity of GC-derived BCRs.

EFhd2 Limits PC Differentiation

Doubling B cell speed in GCs predicted increased GC B cell numbers (Figure 3A). However, we did not register higher numbers of GC B cells or hapten-specific GC B cells at any

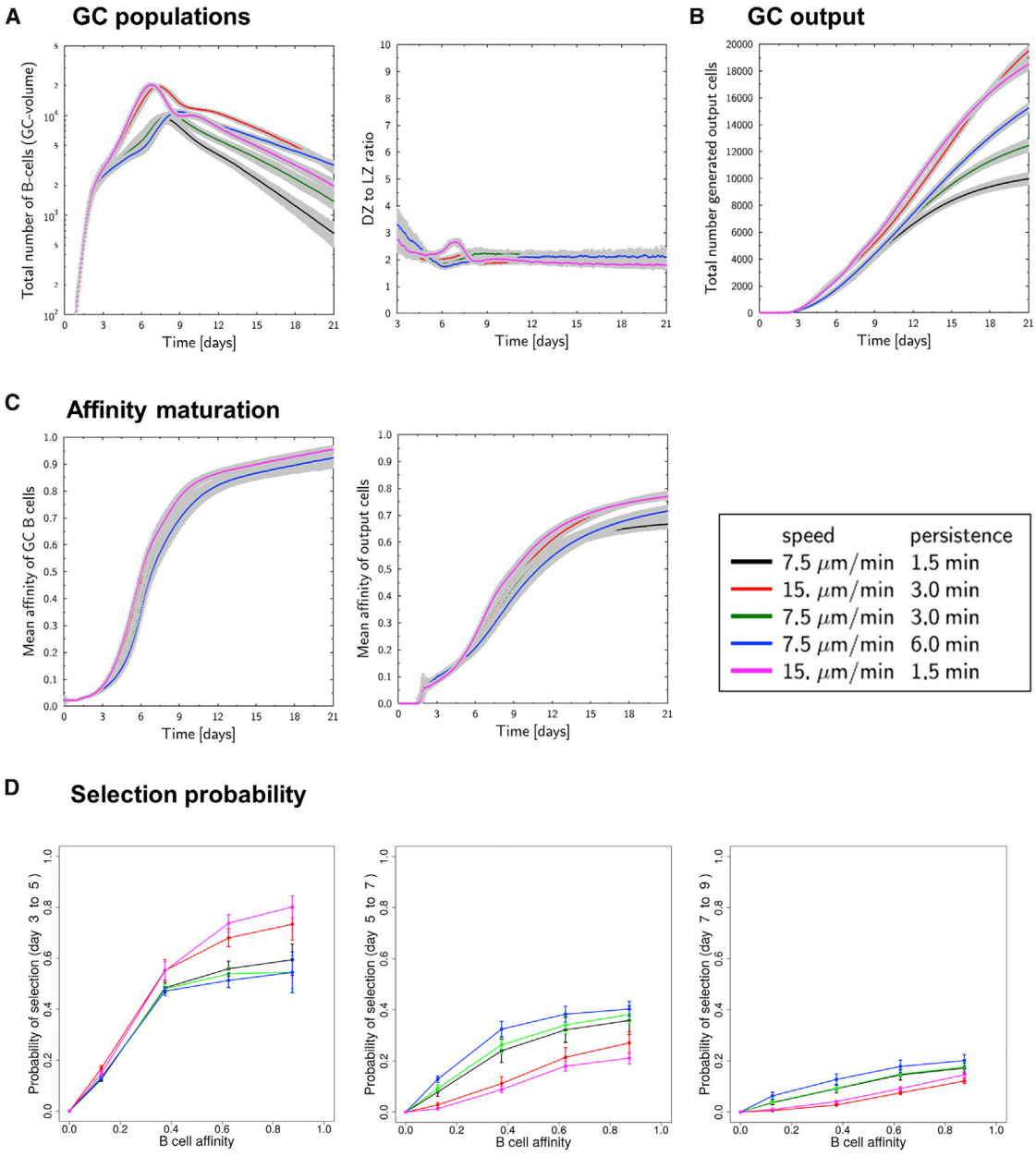

Figure 3. Enhanced B Cell Speed and Persistence Increase GC-Derived PC Output and Affinity

(A and B) *In silico* simulation of GC modulated by speed and persistence B cell migration. Predicted results are shown for the total number of GC B cells, their distribution in dark zone (DZ) and light zone (LZ) (A), and the generation of output cells (B).

(C) Affinity maturation was simulated for GC B cells as well as for the output cells.

(D) The selection probability in dependence of B cell affinity was analyzed for different time points during the GC course.

Data are shown as mean (solid lines) of 50 simulations ± SD (gray shades).

time point between days 7 and 21 upon NP-KLH immunization of EFhd2KO mice (Figures 4A–4C). To test nevertheless whether EFhd2 influences PC generation from GCs, we crossed EFhd2KO mice with Blimp1:GFP reporter mice (Kallies et al., 2004), immunized mice with NP-KLH, and analyzed Blimp1 expression (GFP fluorescence) in $CD38^{low}$ $CD95^{+}$ B cells at day 21. We found a clearly Blimp1-positive cell fraction in $CD19^{+}CD38^{low}CD95$ $GL7^{-}$ cells (Figure 4D). Intriguingly, we detected a higher frequency of Blimp1-positive $CD38^{low}CD95^{+}$ $GL7^{-}$ cells in EFhd2KO mice (Figure 4E), while total cell numbers were hardly elevated (Figure 4F). We explain this by reduced frequencies and numbers of $CD19^{+}CD38^{low}$ B cells in the Blimp1:GFP;EFhd2KO mice (Figures 4G and 4H). In summary, Blimp1-positive late GC B cells are increased in relation to the

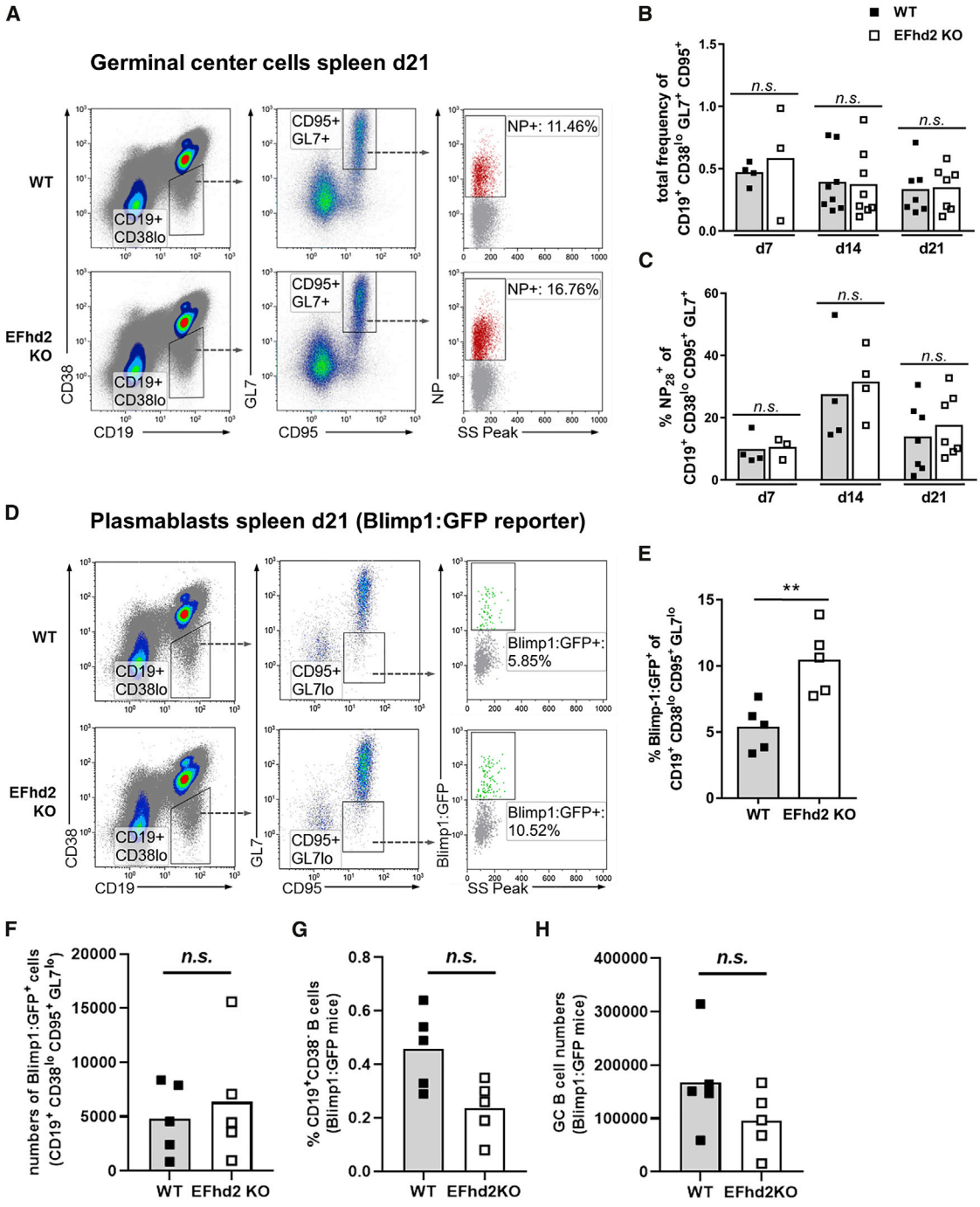

Figure 4. Normal Hapten-Carrier-Induced GC B Cells but Increased GC-Derived PCs in EFhd2-Deficient Mice

(A) WT and EFhd2KO mice were immunized i.p. with 100 μg NP_{29}-KLH in alum and analyzed after 7, 14, and 21 days. Antigen-specific and total GC B cell and PC populations from spleen were determined via fluorescence-activated cell sorting (FACS). Merged FACS dot plots of GC B cells are displayed for day 21, pre-gated on singlets and viable lymphocytes.

(B and C) Frequencies of total GC B cells defined as $CD19^+CD38^{lo}CD95^+GL7^+$ at days 7, 14, and 21 post-immunization. Respective antigen-specific GC B cells, identified by binding to NP_{28}-PE, were quantified as frequency of NP^+ cells of total $CD19^+CD38^{lo}CD95^+GL7^+$ B cells. Data are represented as mean values. Statistics: N = 2, n = 4–8; values passed the test for Gaussian distribution (Shapiro-Wilk normality test), and significance was therefore analyzed using unpaired t test (*n.s.*, $p > 0.05$).

(D) Blimp1:GFP mice and Blimp1:GFP × EFhd2KO mice were immunized i.p. with 100 μg NP_{29}-KLH in alum. Spleens were analyzed for Blimp1:GFP expression of $CD19^+CD38^{lo}CD95^+GL7^{lo}$ B cells by FACS. Merged FACS dot plots of GC-derived PCs are displayed for day 21, pre-gated on singlets and viable lymphocytes.

(legend continued on next page)

frequencies and numbers of $CD19^{+}CD38^{low}$ B cells. These data point to incremented PC generation within EFhd2KO GCs as a consequence of cell migration, which is in agreement with the predictions (Figure 3). If actin-dependent cytoskeletal reorganization can in fact influence PC generation from GCs, then the expression of actin modulating proteins, including EFhd2, should be altered in (1) GCs and (2) the fraction of GC B cells that is predestined to become PCs (fraction 1 in Ise et al., 2018; $Cxcr4^{low}$, $CD86^{+}$, $Bcl6^{low}$, $Irf4^{+}$, and $CD69^{high}$). We therefore analyzed a pre-existing RNA sequencing (RNA-seq) dataset from fraction 1 B cells as well as other GC subsets (Ise et al., 2018; fraction 2: $Cxcr4^{low}$, $CD86^{+}$, $Bcl6^{high}$, $Irf4^{-}$, and $CD69^{int}$; fraction 3: $Cxcr4^{low}$, $CD86^{+}$, $Bcl6^{high}$, and $Irf4^{-}$, $CD69^{low}$; fraction 4: $Cxcr4^{low}$, $CD86^{+}$, $Bcl6^{low}$, $Irf4^{-}$, and $CD69^{low}$; and plasmablasts). These re-analyses showed that genes controlling the B cell actin cytoskeleton, including EFhd2, are sharply regulated at the transition of GC B cells and PCs and strongly enriched in fraction 1 (Figure S3), supporting the idea of an actin-dependent checkpoint in GCs controlling PC development.

EFhd2 Limits Antigen-Specific PC Output from the GC

We next tracked hapten-specific GC B cells, PCs, and serum Abs over 21 days after NP-KLH immunization (Figure 5). Flow cytometry revealed increased NP-specific PC frequencies in the spleen and bone marrow of EFhd2KO mice at day 21 (Figures 5C and 5F). In addition, we observed increased NP-specific serum IgG (of all isotypes; not depicted here), but not IgM Abs (Figures 5G and 5H), in immunized EFhd2KO mice. These results are in agreement with GC simulation and the increase in Blimp1-expressing B cells at day 21 in immunized Blimp1:GFP;EFhd2KO mice (Figure 4A). The increased NP-specific Abs of EFhd2KO mice were dominantly of lower affinity (Figure 5H). The ratio of high- (anti NP(4)-BSA) versus low-affine (anti NP(29)-BSA) Abs that was predicted to be slightly increased was surprisingly not altered. If affinity maturation was severely altered, then NP binding to GC B cells as determined by flow cytometry would be altered as well, which was not the case. Considering that measurement of affinity maturation by ELISA is widely used, these experiments strongly suggest that affinity maturation is not altered in EFhd2KO B cells. Nevertheless, the observed increase in NP-specific Abs appeared to be specific, as we did not observe increased formation of auto-Abs, at least not anti-double stranded DNA Abs (Figure S4). Furthermore, the T-cell-independent type 2 antigen NP-Ficoll did not elicit an increased response in EFhd2KO mice (Figure S4). Thus, several lines of evidence reveal that EFhd2 limits PC generation from GCs, with cell migration limited by EFhd2 likely playing a role therein (Figure 3B). The increase in PCs was not due to increased B cell/T cell interactions as determined by conventional flow as well as Amnis imaging cytometry (Figures S5 and S6) or increased Tfh cell numbers (Figure S7). An *in silico* prediction that was not confirmed in EFhd2KO mice (Figure 4A) was the increase in GC B cells induced by increasing B cell speed or persistence *in silico* (Figure 3A) and an increase in Ab affinity. This raised the possibility that cell migration was not the only parameter altered by EFhd2 deficiency in GC B cells. Since the actin cytoskeleton is also crucial for the B cell/FDC synapse (Tolar, 2017), we next assessed how EFhd2KO B cells interact with FDCs.

EFhd2KO B Cells Have Less Contact with FDCs

To test whether EFhd2KO B cells interact differently with FDCs *in vivo*, we tracked EFhd2KO and WT B cells within the FDC network (Figure 6). The colocalization volume of EFhd2KO B cells with FDCs was reduced (Figure 6B), but the duration of interactions was similar (Figure 6C). However, the B cell/FDC contacts appeared to be more confined on the FDC surface, since the displacement of EFhd2KO B cell contacts was reduced (Figure 6D). We conclude that EFhd2KO GC B cells interact differently with FDCs than WT GC B cells. These data could be explained by altered actin cytoskeleton dynamics.

The Actin Cytoskeleton of EFhd2KO B Cells Is Highly Dynamic

Activated B cells move on ICAM-1 in the presence of Cxcl13 *in vitro* by exhibiting frequent, spontaneous dilation and shrinking events at the sides of the leading membrane edge, which is predictive of turning versus directional persistence (Liu et al., 2016). These conditions are at least partially found on and within the FDC network. The faster migration of BCR-activated EFhd2KO B cells in response to Cxcl13 (Figure 2B) coincided with increased actin dynamics (Figure 6E). We observed specifically that the Uropod (trailing edge; Figure 6F) is stable in WT B cells but highly dynamic in EFhd2KO B cells (see static images in Figure 6E and Videos S2 [WT] and S3 [EFhd2KO]), showing many protrusion-contractile events in EFhd2KO B cells (Figure 6G). We also observed an increased pool of F-actin at the trailing edge of EFhd2KO B cells (Figure 6H).

A Decrease of B-FDC Contact Probability Opposes the GC Increase Induced by High Speed and Persistence

If there was a quantitative or qualitative difference in the B cell/FDC synapses of EFhd2KO B cells, then positive selection could be impaired, reducing the frequency of recycling GC B cells. In this case, the increased GC output predicted to occur when GC B cells migrate faster could be counterbalanced. To reconcile the computer simulation with our experimental data, we changed the likelihood of B cell/FDC interaction as a surrogate

(E) Frequencies of GC-derived PCs defined as $Blimp1^{+}CD19^{+}CD38^{low}CD95^{+}GL7^{low}$ at day 21 post-immunization. Data are represented as mean values. Statistics: N = 2, n = 5; significance was analyzed using Mann-Whitney test (**$p \leq 0.01$).
(F) Absolute numbers of GC-derived PCs defined as $Blimp1^{+}CD19^{+}CD38^{low}CD95^{+}GL7^{low}$ at day 21 post-immunization. Data are represented as mean values. Statistics: N = 2, n = 5; significance was analyzed using Mann-Whitney test.
(G) Frequencies of GC B cells defined as $CD19^{+}CD38^{low}$ at day 21 post-immunization. Data are represented as mean values. Statistics: N = 2, n = 5; significance was analyzed using Mann-Whitney test.
(H) Absolute numbers of GC B cells defined as $CD19^{+}CD38^{low}$ at day 21 post-immunization. Data are represented as mean values. Statistics: N = 2, n = 5; significance was analyzed using Mann-Whitney test.

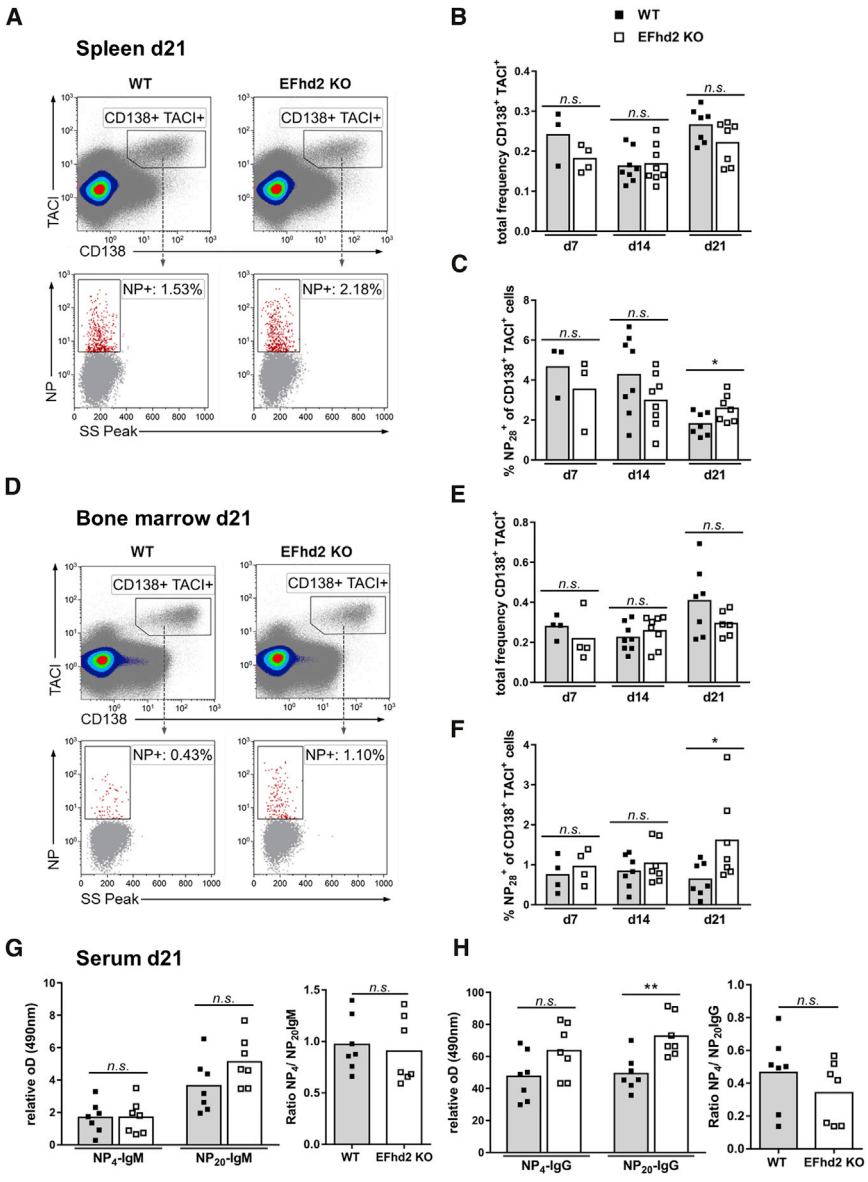

Figure 5. EFhd2 Deficiency Increases Antigen-Specific PC Output without Increasing Ab Affinity

WT and EFhd2KO mice were immunized i.p. with 100 μg NP_{29}-KLH in alum, and spleen and bone marrow were analyzed after 7, 14, and 21 days for antigen-specific and total plasmablast/PC populations via FACS. NP-binding immunoglobulins were detected by serum-ELISA. Merged FACS dot plots are displayed for day 21 for the spleen (A) and bone marrow (BM) (D), pre-gated on singlets and viable lymphocytes. Frequencies of total plasmablasts/PCs defined as $CD138^+TACI^+$ in spleen (B) and bone marrow (E). Antigen-specific plasmablasts/PCs, identified by binding to NP_{28}-PE, were quantified as the frequency of NP^+ cells of total $CD138^+TACI^+$ cells for spleen (C) and bone marrow (F). Sera from day 21 were analyzed for high- and low-affine NP-specific IgM (G) and IgG (H). Data are represented as mean values. Statistics: N = 2, n = 4–8; Shapiro-Wilk and unpaired t test (*n.s.* > 0.05; *p ≤ 0.05; **p ≤ 0.01).

measure for the reduced B cell/FDC contacts we observed (Figure 6B). Decreasing B cell/FDC interaction probability by half indeed completely normalized the elevated GC response elicited by doubled B cell speed (Figure 7A) but did not affect quantitative GC output (Figure 7B), thereby approaching closely the experimental data obtained with EFhd2KO mice immunized with NP-KLH. *In silico*, the reduced antigen uptake led to less intense Tfh cell signals, which induced less division in the DZ and are reflected in a reduced DZ/LZ ratio (Gitlin et al., 2014; Meyer-Hermann, 2014) (Figure 7A). Considering a reduced B cell/FDC interaction probability in the case of simulated doubled B cell persistence instead of doubled B cell speed reduced the increased GC response below the standard setting (Figure 7A), reduced the DZ/LZ ratio even more, and also reduced the increase of GC output (Figure 7B). The higher affinity of GC output cells induced by doubling speed was hardly affected by *in silico* reduction of B cell/FDC interaction but was decreased in the case of doubled persistence (Figure 7C). We conclude that speed and persistence of B cell migration in GCs, along with the propensity to access antigen on FDCs or find supporting stromal cells, are decisive for quantitative and qualitative GC output. How can these theoretical data in turn be validated? In EFhd2KO mice, we did observe increased antigen-specific PC output without an increase in affinity (Figure 5). These data point to a functional consequence of the observed reduced B cell/FDC contacts, which could be reduced positive selection, explaining the phenomenon of increased PC output without increased Ab affinity. Our experiments were performed under noncompetitive conditions, where even B cells without increased BCR affinity may benefit from enhanced migration. To create a competitive situation, we adoptively transferred Ly5.2 EFhd2KO or Ly5.2 WT B cells into Ly5.1 hosts and then immunized the mice and tracked GC B cells. We observed that EFhd2KO B cells are outcompeted at day 21, but not yet at day 14 (Figure S8). A similar finding was also observed in Blimp1:GFP;EFhd2KO mice (Figure 4G). We propose that B cell/FDC contacts are important for GC maintenance when B cells show increased motility under competitive conditions.

DISCUSSION

B cells in GCs that have undergone and survived SHM (Mayer et al., 2017) constantly move to find selective antigen bound on FDCs, cognate Tfh cells, and stromal cell support (Ise et al., 2018; Kräutler et al., 2017; Zhang et al., 2018b), equipping

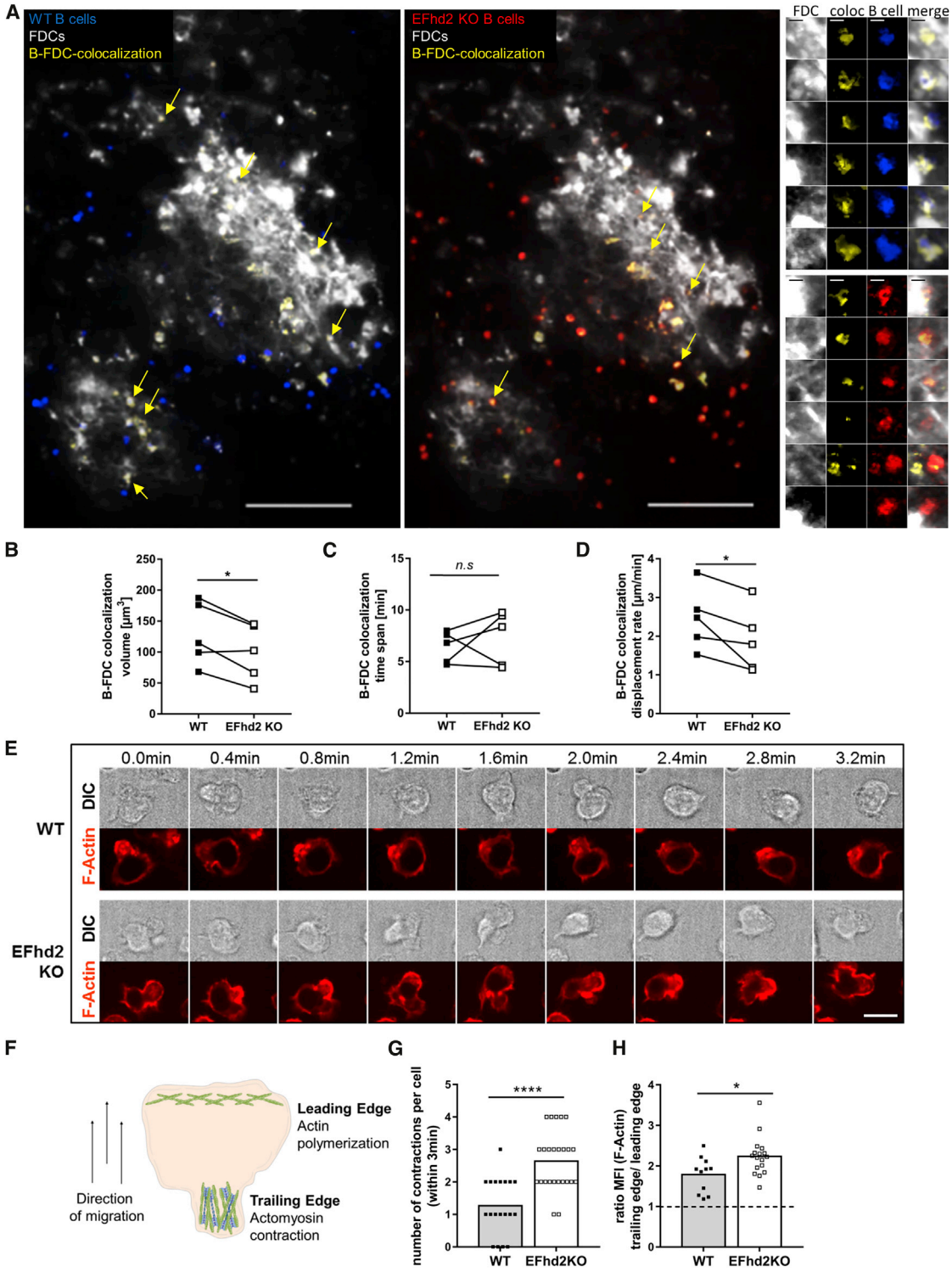

Figure 6. Altered Actin Dynamics and Altered Interaction of EFhd2KO GC B Cells with FDCs

WT and EFhd2KO donor as well as WT recipient mice were immunized i.p. with SRBCs. At day 7, splenic B cells from donor mice were isolated and fluorescently labeled. WT B cells, Hoechst, EFhd2KO B cells, CMTPX, and vice versa, mixed in a 1:1 ratio, were transferred i.v. into WT recipient mice. One day after transfer, the FDC network was labeled via i.v. application of anti-CD21/32-Atto590 Fab_2-Ab. Colocalization of B cells with FDC, motility of B cell/FDC synapses, and B cell/FDC interaction time were assessed.

(legend continued on next page)

them with survival and PC differentiation signals. Lymphocyte movement in lymph nodes observed by two-photon microscopy can best be described as a stochastic (Brownian) walk with persistence of orientation (Meyer-Hermann and Maini, 2005). How different modes of B cell migration in GCs contribute to GC output, in particular PC generation, has to our knowledge not been addressed, although tremendous progress has been made in understanding B cell migration, B cell/FDC interactions, and B cell/T cell interactions (Figge et al., 2008; Meyer-Hermann et al., 2012; Natkanski et al., 2013; Nowosad et al., 2016; Tolar, 2017; Victora and Nussenzweig, 2012). Here, we analyzed intrinsic migration properties of B cells lacking EFhd2 (Brachs et al., 2014). We found a 2-fold increased speed of EFhd2KO B cells in GCs. It was surprising to see EFhd2KO B cells migrating two times faster with unaltered directedness. Liu et al. (2016) have shown that the balance between dilation/shrinking at the edges determines cell migration directionality. I*n vitro*, we did in fact observe more dilation/shrinking events (referred to as "contraction") on both sides of EFhd2KO B cells. We propose that EFhd2KO B cells show unaltered directionality *in vivo* because the increase in cytoskeletal dynamics is balanced between both edges of the migrating cells. We found that the two-times-increased speed of EFhd2KO B cells first proportionally increases GC size and output in the computer simulation and second predicts slightly enhanced affinity of output cells. *In silico*, these effects are associated with higher fractions of B cells in interaction with FDCs and Tfh cells and are associated with faster antigen uptake as well as stronger Tfh cell signaling. Increased PC and hapten-specific IgG, but not increased interactions with FDCs or Tfh cells, were in fact experimentally confirmed in EFhd2KO mice immunized with NP-KLH, as well as with EFhd2KO;Blimp1:GFP reporter mice (Kallies et al., 2004). The Blimp1-positive cells we found at day 21 in the $CD38^{-}CD95^{+}GL7^{low}$ fraction are, according to their CD38 and CD95 expression (Victora et al., 2010), presumably late LZ GC B cells. Radtke and Bannard (2019) identified a Blimp1-positive GC fraction and proposed that those cells are precursors of GC progeny, such as PCs, arising even in the absence of Tfh cells. Our data are consistent with those results, since we did not identify differences in B cell/T cell interactions. Whether the cells we identified are localized in the DZ as well (Radtke and Bannard, 2019) remains to be determined. Although hapten-specific PCs were not elevated at days 7 and 14 in the spleen of NP-KLH immunized EFhd2KO mice, we found more PCs in the bone marrow, arguing for increased homing or residence within the bone marrow. However, more hapten-specific PCs were found in the spleen and bone marrow of immunized EFhd2KO mice at day 21. This points to a late boost in GC-derived PC differentiation consistent with recent data (Weisel et al., 2016) or increased selection pressure as competing Abs in FDC-bound immune complexes increase in affinity over time. Adding more persistence of cell migration on top of higher speed expanded the GC volume *in silico* even more but did not affect GC output or affinity of output cells additionally. In line with previous suggestions made for T cells (Fricke et al., 2016) and current theoretical models (Thomas et al., 2019), we propose that solely increasing speed or directed persistence of migration will increase a B cell's displacement and, thereby, the probability of finding survival signals, leading to enhanced GC reactions as well as enhanced GC output. In EFhd2KO mice, we did observe increased GC output but did not observe increased GC reactions or increased Ab affinity during alum/NP-KLH immunization. We can explain the latter two facts through the reduced B-FDC interactions, but only under noncompetitive conditions where the fast EFhd2KO B cells compete with the equally fast EFhd2KO B cells. Under competitive conditions, we found outcompetition of EFhd2KO GC B cells. Through these transfer experiments of EFhd2KO and WT B cells, we provide experimental evidence for the theoretical model of Thomas et al. (2019), predicting that increased GC B cell migration will lead to a collapse of GCs when B cell proliferation (positive selection) is not increased simultaneously. To what extent downstream signals of positive selection like Myc expression or mTOR activity are affected by loss of EFhd2 requires further investigation. Nevertheless, it appears that B cells integrate not only their location but also different modes of cell migration (speed and persistence) with BCR affinity in GCs, with B cell/FDC contacts playing an important role.

Previously, we observed exacerbated Ab responses by EFhd2KO GC B cells in secondarily *N.-brasiliensis*-infected mixed bone marrow chimeras (Brachs et al., 2014). This finding is in agreement with the increased GC output (i.e., the generation of antigen-specific PC and memory B cells) in our GC computer simulation and EFhd2KO B cells. The strongly T helper type 2 (Th2)-cell-inducing conditions in the *N. brasiliensis* infection model also led to increased EFhd2KO GC B cells (Brachs

(A) Two representative two-photon images of a GC in the spleen showing either WT B cells (blue; left) or EFhd2KO B cells (red; right) in colocalization with FDCs (yellow) (scale bar, 100 μm). The right panel depicts high-magnification images of individual WT and EFhd2KO B cells indicated by yellow arrows in the overview images in (A). For all high-magnification images of B cells, fluorescence of the FDC network (white), fluorescence of B cells (blue, WT B cells; red, EFhd2KO B cells), and the colocalization signal (yellow) are shown both separately and merged (scale bar, 5 μm).
(B) B cell/FDC colocalization volume.
(C) Interaction time of B cells and FDCs.
(D) Displacement rate of B cell/FDC conjugates.
(E) Splenic B cells from WT and EFhd2KO mice were activated with anti IgM-Ab for 48 h, stained with SiR-actin, plated on ICAM-1 in the presence of CXCL13, and analyzed by spinning disc confocal microscopy. Fluorescence and differential interference contrast (DIC) images were taken at indicated time points during a time course of 3.2 min (scale bar, 10 μm).
(F) Schematic of a migrating B cell.
(G) Cytoskeletal dynamics was quantified as number of cell protrusions/contractions within 3 min.
(H) Cellular F-actin distribution was determined as the ratio of the mean fluorescence intensity (MFI) of F-actin (SiR-actin) in the trailing versus the leading edge (schematically illustrated in F). Datasets are shown for individual cells (one dot = one B cell) activated as described above. Statistics: N = 2, n = 2–3; significance was analyzed using Mann-Whitney test (*$p \leq 0.05$; ****$p < 0.0001$).

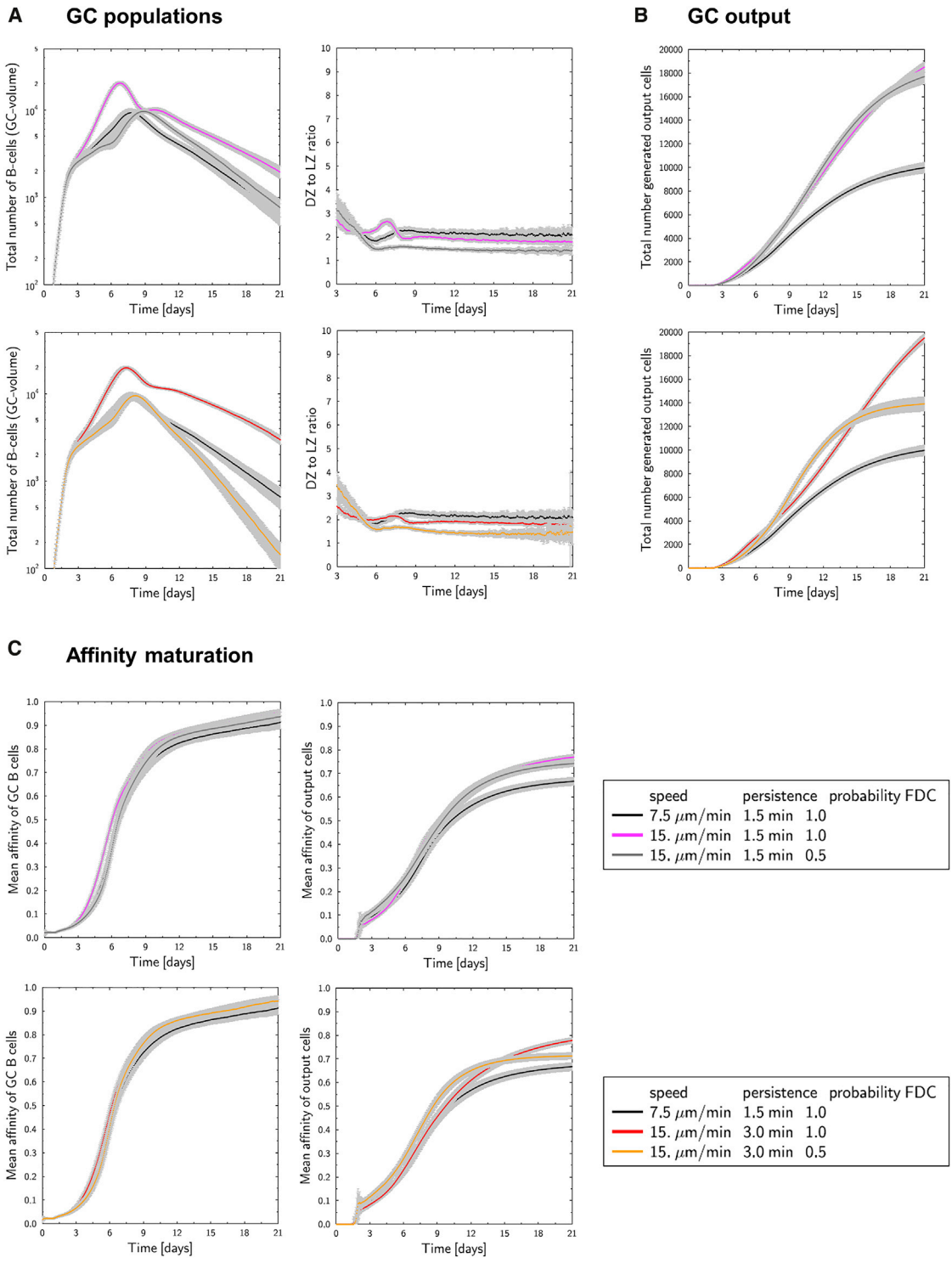

Figure 7. Relationship between Fast and Persistent B Cell Migration with GC Volume, GC-Derived PC Output, and Affinity

In silico simulation of GC modulated by speed and persistence of B cell migration as well as probability of B cell/FDC interaction.

(A and B) Predicted results are shown for the total number of GC B cells, their distribution in DZ and LZ (A), and the generation of output cells (B).

(C) Affinity maturation was simulated for GC B cells as well as for the output cells.

Data are shown as mean (solid lines) of 50 simulations ± SD (gray shades).

et al., 2014), contrary to the NP response we assessed here. EFhd2 is a STAT6 target gene in B cells (Mokada-Gopal et al., 2017), and STAT6 is specifically required for Th2-cell-induced GCs (Turqueti-Neves et al., 2014). Increased GC reactions under specific parasitic Th2 cell and high IL-4 conditions could add to increased PC generation by lack of EFhd2.

It was surprising to observe accelerated B cell migration when B cells lack EFhd2, because EFhd2 was described as a positive regulator of cancer metastases and macrophage immigration into inflamed lung (Fan et al., 2017; Huh et al., 2015; Zhang et al., 2018a). However, leukocytes can migrate rapidly and largely independent of actin stress fibers and integrin-matrix contacts by the sole force of actin-network expansion, which promotes protrusive flowing of the leading edge (Lämmermann et al., 2008). The contribution of EFhd2 to the migration of leukocytes appears thus to be different than its contribution to migration of fibroblast-like cells. The universal-coupling-between-cell-speed-and-cell-persistence (USCP) law (Maiuri et al., 2015) links increased actin retrograde flow to cell migration. As EFhd2KO B cells migrated faster, increased actin retrograde flow is expected. In corroboration of this expectation, we found that migrating EFhd2KO B cells contained more actin at the trailing edge. Our data may be extrapolated to other actin remodeling proteins in B cells, such as Wiskott-Aldrich-interacting protein 1 (WIP1), which is required for persistent cell movement, efficient GC-derived PC generation, and Ab affinity maturation (Keppler et al., 2018). Contrasting the WIP1KO, however, EFhd2KO facilitates PC generation from GCs.

In contrast to the predictions, NP-specific Abs of EFhd2KO mice were not more affine. We considered a second function of EFhd2 in B cells, namely mediating B cell/FDC interactions, and found that EFhd2KO B cells are less (~35%) in contact with FDCs, as defined by measurement of the colocalization volume between B cells and FDCs. This may be a result of increased migration or vice versa, although none of the adhesion molecules assessed on EFhd2KO B cells was differentially expressed. Nevertheless, we conclude that the upregulation of EFhd2 in GC B cells stabilizes B cell/FDC contacts. In line with our finding, EFhd2 stabilizes the CD8 T cell synapse and supports PD-1-mediated T cell suppression *in vitro* (Peled et al., 2018). Based on our previous B-cell-intrinsic results (Brachs et al., 2014), we used total EFhd2KO mice, and this could arguably lead to increased T cell help in GCs. However, we did not detect increased Tfh cell numbers, did not observe more B cell/T cell contacts, and have no evidence for auto-Ab development. Nevertheless, lowering the B cell/FDC interaction probability *in silico* inferred (1) normalization of the increased GC volume elicited by doubled speed; (2) a profound reduction of the persistence-induced escalation of the GC reaction, even below the standard reaction; 3) dampening of the DZ/LZ ratio in the setting of bolstered speed and persistence; (4) reversion of increased GC output under conditions of doubled speed and persistence; and (5) diminishment of the incremented affinity evoked by doubled speed and persistence. We conclude that simulated conditions of doubled speed and an *ad hoc* 0.5 probability of B-FDC contacts describe best the phenotype of EFhd2KO B cells, representing a direct consequence of internal actin dynamics on cellular behavior in a complex environment.

It is tempting to speculate that EFhd2 deficiency may result in a qualitatively different B cell/FDC immune synapse (Nowosad et al., 2016), which, as observed, lasts for the same time but shows less motility. A more efficient synapse may in principle allow even lower affine B cells to access antigen and/or receive adequate BCR signals fostering PC development. Apart from B cells, effective search strategies have evolved in many biological systems. For instance, efficient T cell search is supported not only by directionally persistent migration over defined periods of time but also by heterogeneity and adaptation of movement patterns owing to the microarchitecture of lymph nodes (Fricke et al., 2016). Adaptation of B cell migration within the GC DZ and LZ is coupled to chemokine receptor expression and desensitization (Allen et al., 2004; Gitlin et al., 2014). Cxcr4 desensitization allows PCs to persist stably in the bone marrow niche (Biajoux et al., 2016). We observed more hapten-specific PCs in the bone marrow of EFhd2KO mice. EFhd2 could be involved in sensitization/desensitization of Cxcr4 or Cxcr5, as it can desensitize the G-coupled β2 adrenergic receptor (Nippert et al., 2016). In support, BCR signaling sensitizes EFhd2KO B cells toward Cxcl13. This finding in particular can explain the specific increase in hapten-specific PCs, but not total PCs, over time.

Could the actin cytoskeleton be explored to improve GC responses, or might it even be exploited by pathogens (Spear and Wu, 2014)? Nef (negative regulatory factor), encoded by HIV, perturbs the T cell's actin cytoskeleton independent of chemokine receptor expression and function and interferes with stable cellular polarization required for fast migration (Usmani et al., 2019). Future work may unravel particular GC B-cell-intrinsic and "druggable" enzymatic activities involved in actin remodeling that could be explored as adjuvants. To summarize, based on experimental data, we propose that increased GC B cell displacement through lack of cytoskeletal proteins such as EFhd2 will increase the probability of finding antigen and cognate Tfh cells and therefore contributes to PC development.

STAR★METHODS

Detailed methods are provided in the online version of this paper and include the following:

- KEY RESOURCES TABLE
- RESOURCE AVAILABILITY
  - Lead Contact
  - Materials Availability
  - Data and Code Availability
- EXPERIMENTAL MODEL AND SUBJECT DETAILS
- METHOD DETAILS
  - Two-photon laser-scanning microscopy
  - Analysis of two-photon imaging data
  - Analysis of gene expression data
  - Mice
  - T-dependent immunizations
  - Isolation of primary murine cells from spleen and bone marrow
  - Detection of surface antigens by flow cytometry
  - Enzyme-linked immunosorbent assay (ELISA)
  - Purification of murine B lymphocytes from spleen

- *In vitro* cultivation of primary murine B cells
- *In vitro* migration assay of activated B cells
- Spinning disc confocal microscopy
- Adoptive B cell transfer
- Imaging Cytometry
- *In silico* GC model

● QUANTIFICATION AND STATISTICAL ANALYSIS

SUPPLEMENTAL INFORMATION

Supplemental Information can be found online at https://doi.org/10.1016/j.celrep.2020.108030.

ACKNOWLEDGMENTS

This work was funded by the Deutsche Forschungsgemeinschaft (DFG; transregional collaborative research grant TRR130 to D. Mielenz, A.H., and R.N. and research training grant 1660 to D. Mielenz). We gratefully acknowledge support of the Optical Imaging Center (OICE) of Friedrich Alexander University of Erlangen-Nürnberg and Drs. Kallies and Nutt for Blimp1:GFP reporter mice. We thank Dr. Hans-Martin Jäck for critical reading and the reviewers for their constructive comments.

AUTHOR CONTRIBUTIONS

D.R., A.R., T.S., P.T., J.T., M.B., S.U., R.A.N., and D. Mielenz performed experiments. M.M.-H. performed the computer simulations. D.R., M.M.-H, A.E.H., R.A.N., and D. Mielenz designed experiments. D.R., M.M.-H., P.T., R.A.N., S.R.S., M.B., and D. Mielenz analyzed data. S.R.S. performed bioinformatics analyses. D.R., M.M.-H., M.B., A.E.H., R.A.N., and D. Mielenz wrote the paper. D. Mougiakakos provided intellectual and infrastructural help.

DECLARATION OF INTERESTS

The authors declare no competing interests.

Received: September 6, 2019
Revised: April 15, 2020
Accepted: July 22, 2020
Published: August 11, 2020

REFERENCES

Allen, C.D., Ansel, K.M., Low, C., Lesley, R., Tamamura, H., Fujii, N., and Cyster, J.G. (2004). Germinal center dark and light zone organization is mediated by CXCR4 and CXCR5. Nat. Immunol. *5*, 943–952.

Allen, C.D., Okada, T., Tang, H.L., and Cyster, J.G. (2007). Imaging of germinal center selection events during affinity maturation. Science *315*, 528–531.

Beltman, J.B., Allen, C.D., Cyster, J.G., and de Boer, R.J. (2011). B cells within germinal centers migrate preferentially from dark to light zone. Proc. Natl. Acad. Sci. USA *108*, 8755–8760.

Berek, C., Berger, A., and Apel, M. (1991). Maturation of the immune response in germinal centers. Cell *67*, 1121–1129.

Biajoux, V., Natt, J., Freitas, C., Alouche, N., Sacquin, A., Hemon, P., Gaudin, F., Fazilleau, N., Espéli, M., and Balabanian, K. (2016). Efficient plasma cell differentiation and trafficking require Cxcr4 desensitization. Cell Rep. *17*, 193–205.

Binder, S.C., and Meyer-Hermann, M. (2016). Implications of intravital imaging of murine germinal centers on the control of B cell selection and division. Front. Immunol. *7*, 593.

Brachs, S., Turqueti-Neves, A., Stein, M., Reimer, D., Brachvogel, B., Bösl, M., Winkler, T., Voehringer, D., Jäck, H.M., and Mielenz, D. (2014). Swiprosin-1/EFhd2 limits germinal center responses and humoral type 2 immunity. Eur. J. Immunol. *44*, 3206–3219.

Calado, D.P., Sasaki, Y., Godinho, S.A., Pellerin, A., Köchert, K., Sleckman, B.P., de Alborán, I.M., Janz, M., Rodig, S., and Rajewsky, K. (2012). The cell-cycle regulator c-Myc is essential for the formation and maintenance of germinal centers. Nat. Immunol. *13*, 1092–1100.

Carrasco, Y.R., Fleire, S.J., Cameron, T., Dustin, M.L., and Batista, F.D. (2004). LFA-1/ICAM-1 interaction lowers the threshold of B cell activation by facilitating B cell adhesion and synapse formation. Immunity *20*, 589–599.

Dogan, I., Bertocci, B., Vilmont, V., Delbos, F., Mégret, J., Storck, S., Reynaud, C.A., and Weill, J.C. (2009). Multiple layers of B cell memory with different effector functions. Nat. Immunol. *10*, 1292–1299.

Dütting, S., Brachs, S., and Mielenz, D. (2011). Fraternal twins: Swiprosin-1/EFhd2 and Swiprosin-2/EFhd1, two homologous EF-hand containing calcium binding adaptor proteins with distinct functions. Cell Commun. Signal. *9*, 2.

Fan, C.C., Cheng, W.C., Huang, Y.C., Sher, Y.P., Liou, N.J., Chien, Y.C., Lin, P.S., Lin, P.S., Chen, C.H., and Chang, W.C. (2017). EFHD2 promotes epithelial-to-mesenchymal transition and correlates with postsurgical recurrence of stage I lung adenocarcinoma. Sci. Rep. *7*, 14617.

Figge, M.T., Garin, A., Gunzer, M., Kosco-Vilbois, M., Toellner, K.M., and Meyer-Hermann, M. (2008). Deriving a germinal center lymphocyte migration model from two-photon data. J. Exp. Med. *205*, 3019–3029.

Fricke, G.M., Letendre, K.A., Moses, M.E., and Cannon, J.L. (2016). Persistence and adaptation in immunity: T cells balance the extent and thoroughness of search. PLoS Comput. Biol. *12*, e1004818.

Gatto, D., and Brink, R. (2010). The germinal center reaction. J. Allergy Clin. Immunol. *126*, 898–907, quiz 908–909.

Gitlin, A.D., Shulman, Z., and Nussenzweig, M.C. (2014). Clonal selection in the germinal centre by regulated proliferation and hypermutation. Nature *509*, 637–640.

Hagen, S., Brachs, S., Kroczek, C., Fürnrohr, B.G., Lang, C., and Mielenz, D. (2012). The B cell receptor-induced calcium flux involves a calcium mediated positive feedback loop. Cell Calcium *51*, 411–417.

Hauser, A.E., Junt, T., Mempel, T.R., Sneddon, M.W., Kleinstein, S.H., Henrickson, S.E., von Andrian, U.H., Shlomchik, M.J., and Haberman, A.M. (2007). Definition of germinal-center B cell migration in vivo reveals predominant intrazonal circulation patterns. Immunity *26*, 655–667.

Heinig, K., Gätjen, M., Grau, M., Stache, V., Anagnostopoulos, I., Gerlach, K., Niesner, R.A., Cseresnyes, Z., Hauser, A.E., Lenz, P., et al. (2014). Access to follicular dendritic cells is a pivotal step in murine chronic lymphocytic leukemia B-cell activation and proliferation. Cancer Discov. *4*, 1448–1465.

Heise, N., De Silva, N.S., Silva, K., Carette, A., Simonetti, G., Pasparakis, M., and Klein, U. (2014). Germinal center B cell maintenance and differentiation are controlled by distinct NF-κB transcription factor subunits. J. Exp. Med. *211*, 2103–2118.

Huh, Y.H., Kim, S.H., Chung, K.-H., Oh, S., Kwon, M.-S., Choi, H.-W., Rhee, S., Ryu, J.-H., Park, Z.Y., Jun, C.-D., and Song, W.K. (2013). Swiprosin-1 modulates actin dynamics by regulating the F-actin accessibility to cofilin. Cell. Mol. Life Sci. *70*, 4841–4854.

Huh, Y.H., Oh, S., Yeo, Y.R., Chae, I.H., Kim, S.H., Lee, J.S., Yun, S.J., Choi, K.Y., Ryu, J.H., Jun, C.D., and Song, W.K. (2015). Swiprosin-1 stimulates cancer invasion and metastasis by increasing the Rho family of GTPase signaling. Oncotarget *6*, 13060–13071.

Ise, W., Fujii, K., Shiroguchi, K., Ito, A., Kometani, K., Takeda, K., Kawakami, E., Yamashita, K., Suzuki, K., Okada, T., et al. (2018). T follicular helper cell-germinal center B cell interaction strength regulates entry into plasma cell or recycling germinal center cell fate. Immunity *48*, 702–715.e704.

Kallies, A., Hasbold, J., Tarlinton, D.M., Dietrich, W., Corcoran, L.M., Hodgkin, P.D., and Nutt, S.L. (2004). Plasma cell ontogeny defined by quantitative changes in blimp-1 expression. J. Exp. Med. *200*, 967–977.

Kepler, T.B., and Perelson, A.S. (1993). Cyclic re-entry of germinal center B cells and the efficiency of affinity maturation. Immunol. Today *14*, 412–415.

Keppler, S.J., Burbage, M., Gasparrini, F., Hartjes, L., Aggarwal, S., Massaad, M.J., Geha, R.S., Bruckbauer, A., and Batista, F.D. (2018). The lack of WIP

binding to actin results in impaired B cell migration and altered humoral immune responses. Cell Rep. *24*, 619–629.

Klein, U., Casola, S., Cattoretti, G., Shen, Q., Lia, M., Mo, T., Ludwig, T., Rajewsky, K., and Dalla-Favera, R. (2006). Transcription factor IRF4 controls plasma cell differentiation and class-switch recombination. Nat. Immunol. *7*, 773–782.

Kolde, R. (2015). Pheatmap: Pretty Heatmaps. R package (version 108) (R Foundation for Statistical Computing).

Kräutler, N.J., Suan, D., Butt, D., Bourne, K., Hermes, J.R., Chan, T.D., Sundling, C., Kaplan, W., Schofield, P., Jackson, J., et al. (2017). Differentiation of germinal center B cells into plasma cells is initiated by high-affinity antigen and completed by Tfh cells. J. Exp. Med. *214*, 1259–1267.

Kroczek, C., Lang, C., Brachs, S., Grohmann, M., Dütting, S., Schweizer, A., Nitschke, L., Feller, S.M., Jäck, H.M., and Mielenz, D. (2010). Swiprosin-1/EFhd2 controls B cell receptor signaling through the assembly of the B cell receptor, Syk, and phospholipase C gamma2 in membrane rafts. J. Immunol. *184*, 3665–3676.

Kwon, M.-S., Park, K.R., Kim, Y.-D., Na, B.-R., Kim, H.-R., Choi, H.-J., Piragyte, I., Jeon, H., Chung, K.H., Song, W.K., et al. (2013). Swiprosin-1 is a novel actin bundling protein that regulates cell spreading and migration. PLoS ONE *8*, e71626.

Lämmermann, T., Bader, B.L., Monkley, S.J., Worbs, T., Wedlich-Söldner, R., Hirsch, K., Keller, M., Förster, R., Critchley, D.R., Fässler, R., and Sixt, M. (2008). Rapid leukocyte migration by integrin-independent flowing and squeezing. Nature *453*, 51–55.

Lee, A.Y.S., Reimer, D., Zehrer, A., Lu, M., Mielenz, D., and Körner, H. (2017). Expression of membrane-bound CC chemokine ligand 20 on follicular T helper cells in T-B-cell conjugates. Front. Immunol. *8*, 1871.

Liu, X., Asokan, S.B., Bear, J.E., and Haugh, J.M. (2016). Quantitative analysis of B-lymphocyte migration directed by CXCL13. Integr. Biol. *8*, 894–903.

Luo, W., Weisel, F., and Shlomchik, M.J. (2018). B cell receptor and CD40 signaling are rewired for synergistic induction of the c-Myc transcription factor in germinal center B cells. Immunity *48*, 313–326.e315.

Maiuri, P., Rupprecht, J.F., Wieser, S., Ruprecht, V., Bénichou, O., Carpi, N., Coppey, M., De Beco, S., Gov, N., Heisenberg, C.P., et al. (2015). Actin flows mediate a universal coupling between cell speed and cell persistence. Cell *161*, 374–386.

Masuzzo, P., Van Troys, M., Ampe, C., and Martens, L. (2016). Taking aim at moving targets in computational cell migration. Trends Cell Biol. *26*, 88–110.

Mayer, C.T., Gazumyan, A., Kara, E.E., Gitlin, A.D., Golijanin, J., Viant, C., Pai, J., Oliveira, T.Y., Wang, Q., Escolano, A., et al. (2017). The microanatomic segregation of selection by apoptosis in the germinal center. Science *358*, 358.

Meyer-Hermann, M. (2014). Overcoming the dichotomy of quantity and quality in antibody responses. J. Immunol. *193*, 5414–5419.

Meyer-Hermann, M.E., and Maini, P.K. (2005). Interpreting two-photon imaging data of lymphocyte motility. Phys. Rev. E Stat. Nonlin. Soft Matter Phys. *71*, 061912.

Meyer-Hermann, M., Figge, M.T., and Toellner, K.M. (2009). Germinal centres seen through the mathematical eye: B-cell models on the catwalk. Trends Immunol. *30*, 157–164.

Meyer-Hermann, M., Mohr, E., Pelletier, N., Zhang, Y., Victora, G.D., and Toellner, K.M. (2012). A theory of germinal center B cell selection, division, and exit. Cell Rep. *2*, 162–174.

Meyer-Hermann, M., Binder, S.C., Mesin, L., and Victora, G.D. (2018). Computer simulation of multi-color brainbow staining and clonal evolution of B cells in germinal centers. Front. Immunol. *9*, 2020.

Mokada-Gopal, L., Boeser, A., Lehmann, C.H.K., Drepper, F., Dudziak, D., Warscheid, B., and Voehringer, D. (2017). Identification of novel STAT6-regulated proteins in mouse B cells by comparative transcriptome and proteome analysis. J. Immunol. *198*, 3737–3745.

Natkanski, E., Lee, W.Y., Mistry, B., Casal, A., Molloy, J.E., and Tolar, P. (2013). B cells use mechanical energy to discriminate antigen affinities. Science *340*, 1587–1590.

Nippert, F., Schreckenberg, R., Hess, A., Weber, M., and Schlüter, K.D. (2016). The effects of Swiprosin-1 on the formation of pseudopodia-like structures and β-adrenoceptor coupling in cultured adult rat ventricular cardiomyocytes. PLoS ONE *11*, e0167655.

Nowosad, C.R., Spillane, K.M., and Tolar, P. (2016). Germinal center B cells recognize antigen through a specialized immune synapse architecture. Nat. Immunol. *17*, 870–877.

O'Connor, M.J., Hauser, A.E., Haberman, A.M., and Kleinstein, S.H. (2011). Activated germinal centre B cells undergo directed migration. Int. J. Data Min. Bioinform. *5*, 321–331.

Peled, M., Dragovich, M.A., Adam, K., Strazza, M., Tocheva, A.S., Vega, I.E., and Mor, A. (2018). EF hand domain family member D2 is required for T cell cytotoxicity. J. Immunol. *201*, 2824–2831.

Radtke, D., and Bannard, O. (2019). Expression of the plasma cell transcriptional regulator Blimp-1 by dark zone germinal center B cells during periods of proliferation. Front. Immunol. *9*, 3106.

Rakhymzhan, A., Leben, R., Zimmermann, H., Günther, R., Mex, P., Reismann, D., Ulbricht, C., Acs, A., Brandt, A.U., Lindquist, R.L., et al. (2017). Synergistic strategy for multicolor two-photon microscopy: application to the analysis of germinal center reactions in vivo. Sci. Rep. *7*, 7101.

Reinhardt, R.L., Liang, H.E., and Locksley, R.M. (2009). Cytokine-secreting follicular T cells shape the antibody repertoire. Nat. Immunol. *10*, 385–393.

Rolink, A., Melchers, F., and Andersson, J. (1996). The SCID but not the RAG-2 gene product is required for S mu-S epsilon heavy chain class switching. Immunity *4*, 319–330.

Schwickert, T.A., Lindquist, R.L., Shakhar, G., Livshits, G., Skokos, D., Kosco-Vilbois, M.H., Dustin, M.L., and Nussenzweig, M.C. (2007). In vivo imaging of germinal centres reveals a dynamic open structure. Nature *446*, 83–87.

Spear, M., and Wu, Y. (2014). Viral exploitation of actin: force-generation and scaffolding functions in viral infection. Virol. Sin. *29*, 139–147.

Thomas, M.J., Klein, U., Lygeros, J., and Rodríguez Martínez, M. (2019). A probabilistic model of the germinal center reaction. Front. Immunol. *10*, 689.

Tolar, P. (2017). Cytoskeletal control of B cell responses to antigens. Nat. Rev. Immunol. *17*, 621–634.

Tu, Y., Zhang, L., Tong, L., Wang, Y., Zhang, S., Wang, R., Li, L., and Wang, Z. (2018). EFhd2/swiprosin-1 regulates LPS-induced macrophage recruitment via enhancing actin polymerization and cell migration. Int. Immunopharmacol. *55*, 263–271.

Turqueti-Neves, A., Otte, M., Prazeres da Costa, O., Höpken, U.E., Lipp, M., Buch, T., and Voehringer, D. (2014). B-cell-intrinsic STAT6 signaling controls germinal center formation. Eur. J. Immunol. *44*, 2130–2138.

Usmani, S.M., Murooka, T.T., Deruaz, M., Koh, W.H., Sharaf, R.R., Di Pilato, M., Power, K.A., Lopez, P., Hnatiuk, R., Vrbanac, V.D., et al. (2019). HIV-1 balances the fitness costs and benefits of disrupting the host cell actin cytoskeleton early after mucosal transmission. Cell Host Microbe *25*, 73–86.e75.

Victora, G.D., and Nussenzweig, M.C. (2012). Germinal centers. Annu. Rev. Immunol. *30*, 429–457.

Victora, G.D., Schwickert, T.A., Fooksman, D.R., Kamphorst, A.O., Meyer-Hermann, M., Dustin, M.L., and Nussenzweig, M.C. (2010). Germinal center dynamics revealed by multiphoton microscopy with a photoactivatable fluorescent reporter. Cell *143*, 592–605.

Weisel, F.J., Zuccarino-Catania, G.V., Chikina, M., and Shlomchik, M.J. (2016). A temporal switch in the germinal center determines differential output of memory B and plasma cells. Immunity *44*, 116–130.

Zhang, S., Tu, Y., Sun, Y.M., Li, Y., Wang, R.M., Cao, Y., Li, L., Zhang, L.C., and Wang, Z.B. (2018a). Swiprosin-1 deficiency impairs macrophage immune response of septic mice. JCI Insight *3*, e95396.

Zhang, Y., Tech, L., George, L.A., Acs, A., Durrett, R.E., Hess, H., Walker, L.S.K., Tarlinton, D.M., Fletcher, A.L., Hauser, A.E., and Toellner, K.M. (2018b). Plasma cell output from germinal centers is regulated by signals from Tfh and stromal cells. J. Exp. Med. *215*, 1227–1243.

STAR★METHODS

KEY RESOURCES TABLE

REAGENT or RESOURCE	SOURCE	IDENTIFIER
Antibodies		
Anti CD16/32, clone 93	Biolegend	# 101302, RRID:AB_312801
Anti TACI/CD267 (APC, clone eBio8F10-3)	eBioscience	Cat# 17-5942-82, RRID:AB_842758
Anti Ly5.2/CD45.2 (PerCPCy5.5, clone 104)	eBioscience	Cat# 35-0454-82, RRID:AB_469725
Anti CXCR4/CD184 (PE, clone 2b11)	eBioscience	Cat# 12-9991-82, RRID:AB_891391
Anti CD19 (BV421/ APCFire750, clone 6D5)	Biolegend	Cat# 115558, RRID:AB_2572120
Anti CD38 (PerCPCy5.5, clone 90)	Biolegend	Cat# 102722, RRID:AB_2563333
Anti CD138 (PECy7, clone 281-2)	Biolegend	Cat# 142513, RRID:AB_2562197
Anti Ly5.1/CD45.1 (PB or PECy7, clone A20)	Biolegend	Cat# 110730, RRID:AB_1134168
Anti CXCR5/CD185 (Biotin or PEDazzle, clone L138D7)	Biolegend	Cat# 145509, RRID:AB_2562125
Anti VLA-4/CD49d-CD29 (PerCPCy5.5, clone R1-2)	Biolegend	Cat# 103619, RRID:AB_2563701
Anti ICAM-2/CD102 (AF488, clone 3C4)	Biolegend	Cat# 105609, RRID:AB_2264501
Anti LFA-1/CD11a (AF488, clone M17/4)	Biolegend	Cat# 101111, RRID:AB_493432
Anti GL-7 (AF647, clone GL-7)	BD Biosciences	Cat# 561529
Anti CD95 (PECy7, clone Jo2),	BD Biosciences	Cat# 554254, RRID:AB_395326
Anti ICAM-1/CD54 (APC, clone 3E2)	BD Biosciences	Cat# 561605
Anti CD4 (FITC, clone gk1.5)	BD Biosciences	Cat# 561828
Anti CD21/35 (clone 8C12)	BD Biosciences	Cat# 558768, RRID:AB_397114
Goat anti mouse IgM-HRP	Southern Biotech	Cat# 1021-05
Goat anti mouse IgG-HRP	Southern Biotech	Cat# 1030-05
Goat anti-IgM AffiniPure F(ab')$_2$ μ chain specific	Jackson ImmunoResearch	Cat# 115-006-020, RRID:AB_2338469
Anti CD40, clone FGK45,	Rolink et al., 1996	RRID:AB_2490239
Chemicals, Peptides, and Recombinant Proteins		
4-Hydroxy-3-nitrophenylacetyl (Phycoerythrin)	Biosearch Technologies.	Cat# N-5070
4-Hydroxy-3-nitrophenylacetyl (keyhole limpet hemocyanin)	Biosearch Technologies.	Cat# N-5060
4-Hydroxy-3-nitrophenylacetyl (bovine serum albumin)	Biosearch Technologies.	Cat# N-5050
Hoechst 33342	Sigma	Cat# B2261
CellTracker Red CMTPX	Thermo Fisher	Cat# C34552
Imject Alum	Thermo Fisher	Cat# 77161
Poly-L-Lysine	Sigma	Cat# P8920
Calf thymus DNA	Sigma	Cat# D1501
Interleukin-4, premium grade	Miltenyi Biotech	Cat# 130-097-761
Cxcl12, carrier free	Biolegend	Cat# 581204
Cxcl13, carrier free	Biolegend	Cat# 583904
Fatty acid free BSA	Sigma	Cat# A8806
Protein A	Sigma	Cat# P6031
Protein A Sepharose	Thermo Scientific	Cat# 101041
SiR-actin	Spirochrome	Cat# SC001
Streptavidin (Cy5)	Jackson ImmunoResearch	Cat# 016-170-084
Critical Commercial Assays		
EasySep B cell isolation kit	Stem Cell Technologies	Cat#19854
Experimental Models: Cell Lines		
293 cells	ATCC	Cat# CRL-1573, RRID:CVCL_0045

(*Continued on next page*)

Continued

REAGENT or RESOURCE	SOURCE	IDENTIFIER
Experimental Models: Organisms/Strains		
Ly5.1 (B6.SJL-Ptprc^{a} Pepc^{b}/BoyJ) mice	Jackson Laboratories	Cat# JAX:002014, RRID:IMSR_JAX:002014
EFhd2KO (Efhd2$^{tm1(KOMP)Vlcg}$) mice	Brachs et al., 2014	MGI # 5707812, RRID:MGI:5707812
Blimp1:GFP (B6/Prdm1^{tm1Nutt}) mice	Kallies et al., 2004	MGI# 3510704
Oligonucleotides		
ICAM-1Fcfwd tgtcacgaattcgcaggtatccatccatcccagagaag	Invitrogen; this study	N/A
ICAM-1Fcrev atgcagatctgttattttgagagtggtacagt	Invitrogen; this study	N/A
Recombinant DNA		
pFUSE-rIgG-Fc2	Invivogen	Cat# pfuse-rfc1
pFUSE-rIgG-Fc2-ICAM1	Addgene; this study	Addgene ID 156462
Software and Algorithms		
GraphPad Prism	Graphpad	https://www.graphpad.com/scientific-software/prism/
Imaris	Oxford Instruments	https://imaris.oxinst.com/
Volocity	Quorum technologies	https://quorumtechnologies.com/volocity
R Pheatmaps	Kolde, 2015	https://cran.r-project.org/web/packages/pheatmap/index.html
Shortest path algorithm	Rakhymzhan et al., 2017	N/A
Kaluza	Beckman Coulter	https://www.beckman.de/flow-cytometry/software/kaluza
Other		
μ slide 8-well polymer chambered coverslips	Ibidi Bioscience	Cat# 80826
Sheep red blood cells	Fiebig Nährstofftechnik	Cat# 31100100

RESOURCE AVAILABILITY

Lead Contact

Further information and requests for resources and reagents should be directed to and will be fulfilled by the Lead Contact Dirk Mielenz (dirk.mielenz@fau.de)

Materials Availability

All unique reagents generated in this study are available from the Lead Contact. The plasmid pFuse-rIgG–Fc2-ICAM1 generated in this study has been deposited to Addgene. The accession number for pFuse-rIgG–Fc2-ICAM1 Addgene: 156462.

Data and Code Availability

This study did not generate new resource datasets or code.

EXPERIMENTAL MODEL AND SUBJECT DETAILS

All experimental procedures were done in agreement with animal protocols approved by the Government of Lower Franconia, Bavaria, Germany. Both female and male mice were used in the experiments. Mice were maintained on a 12-h light/dark cycle with free access to food and water according to governmental rules. The Blimp1:GFP (B6/Prdm1^{tm1Nutt}) and EFhd2KO (Efhd2$^{tm1(KOMP)Vlcg}$) mice used in this study were described previously (Brachs et al., 2014; Kallies et al., 2004). All mice were in C57BL/6 backgrounds and between 8-12 weeks old. Sex matched littermates or age and sex matched animals were used as controls.

METHOD DETAILS

Two-photon laser-scanning microscopy

All imaging experiments of *ex vivo* spleen slices were performed using a specialized multi-photon laser-scanning microscope based on a commercial scan head (TriMScope II, LaVision BioTec, Bielefeld, Germany) previously described (Rakhymzhan et al., 2017). The detection of the fluorescence signals was accomplished with photomultiplier tubes in the ranges 460 ± 30 nm (Hoechst), 525 ± 25 nm (autofluorescence), 593 ± 20 nm (CMTPX) and 655 ± 20 nm (CD21/35-Fab-Alexa 647). The excitation of Hoechst, CMTPX and Alexa

647 was performed at 850 nm of Ti:Sa laser and 1100 nm of OPO. In all experiments, we focused the laser beams with an 20x objective lens (Apochromat water-immersion, NA = 1.0, WD = 2 mm, Zeiss, Jena, Germany) and maximally used an average laser power of 8 mW to avoid photodamage. The pulse width of the Ti:Sa beam amounted to 160 fs, that of the OPO beam to 150 fs, under the objective lens.

Analysis of two-photon imaging data

All time-lapse 3D fluorescence data acquired in spleen slices by two-photon microscopy were loaded either in Imaris (BitPlane) or Volocity (Quorum technologies), post-processed with a Gaussian-filter to reduce signal noise and contrasted for best image quality. The objects in each spectral channel of the 4D data were segmented using a standardized automatic pipeline based on the watershed algorithm. The pipeline relies on signal discrimination using the measure of local signal-to-background ratio followed by object merging or separation according to the expected average cell volume. The segmentation results were subsequently inspected by the researchers to exclude non-sense segmentation. After this step, we determined cell numbers and volume. For object tracking over time we used the shortest-path-algorithm, which was previously demonstrated to reliably perform for the used fluorescent cell concentration per imaged volume unit (Rakhymzhan et al., 2017). Also the tracking results were subsequently inspected to exclude artifacts. The results of this step were for each cell: 1) time period the cell could be monitored (time span), 2) position (x,y,z) to each time point. Based on this information the 3) track length (distance), 4) displacement length (displacement), 5) immediate velocity to each time point, 6) average velocity for the whole time span (velocity), 7) displacement rate averaged for the whole time span (displacement rate) and 8) directedness as the ratio between displacement length and track length were determined. Cell-cell contacts were quantified by measuring the colocalization of the corresponding spectral channels, chosen to have a minimum cross-talk. Colocalization is defined as overlap of two spectral signals measured in each pixel. Discrimination between signal and background was performed relying on local signal-to-background ratio. The same segmentation pipeline and tracking algorithm as described for cells were used to identify and follow cell-cell contact objects over time.

Analysis of gene expression data

Heatmaps of normalized expression values derived from publicly available gene expression data based on RNA Seq (Ise et al., 2018) were generated using the R heatmaps package (Kolde, 2015).

Mice

Constitutively EFhd2 deficient mice (EFhd2KO) on a C57BL/6 background were described previously (Brachs et al., 2014). Blimp1:GFP reporter mice were kindly provided by Stephen Nutt (Kallies et al., 2004) and crossed to EFhd2KO mice. Ly5.1 (B6.SJL-Ptprc^{a} Pepc^{b}/BoyJ) mice were bought from The Jackson Laboratory. Mice were used at 8–12 weeks of age, wild-type (WT) littermates or age and sex matched animals from the same facility served as controls. Mice were kept under pathogen free conditions in the IVC of the Franz-Penzoldt-Center (Erlangen, Germany), experiments were performed according to ethical guidelines for animal experimentation under control of the government of Lower Franconia, Bavaria, Germany.

T-dependent immunizations

Mice were injected with 100μg NP_{29}-KLH (Biosearch Technologies) in Alum (ThermoScientific) in a 1:2 ratio (200μl total volume) or with 2x10^{9} sheep red blood cells (SRBCs, Fiebig Nährstofftechnik) in 200μl PBS intraperitoneally (i.p.).

Isolation of primary murine cells from spleen and bone marrow

Spleen was transferred in cold R10 medium (RPMI 1640, 10% FCS, 2mM glutamate, 1mM sodium pyruvate, 50 U/ml penicillin G, 50 μg/ml streptomycin, 50 μM β-mercaptoethanol) and gently passed through a 70μm cell strainer (BD) using the plunger of a 5ml syringe (BD). Femur and tibia were flushed with cold R10 medium using a 27G cannula (BD). Cell suspensions were pelleted by centrifugation at 300xg for 5min at 4°C. Erythrocytes were lysed upon resuspension in red blood cell-lysis buffer (150mM NH_4Cl, 10mM $KHCO_3$, 100μM EDTA) for 5min at room temperature. The reaction was stopped by adding cold R10 medium before centrifugation at 300xg for 5min at 4°C. The final cell suspensions were kept in cold R10 medium after filtration through 30μm mesh filter (Sysmex).

Detection of surface antigens by flow cytometry

2x10^{6}- 4x10^{6} cells were pelleted in FACS tubes (Micronic) at 300xg for 5min at 4°C and resuspended in 50μl of unlabeled anti-CD16/32 Ab (10 μg/ml in FACS-buffer (PBS, 2%FCS, 0.05% sodium azide)) for 15min on ice. Cells were washed once with FACS-buffer by centrifugation at 300xg for 5min at 4°C, resuspended in 50μl FACS-buffer containing the respective fluorochrome-coupled Abs and incubated for 20min on ice in the dark. Cells were washed twice with FACS-buffer by centrifugation at 300xg for 5min at 4°C. Data were acquired using a Gallios flow cytometer (Beckman Coulter). Analyses were performed using Kaluza version 1.3 and 2.1 (Beckman Coulter). Abs and other reagents are described in the key resources table.

Enzyme-linked immunosorbent assay (ELISA)

Serum samples from NP-KLH immunized mice (see above) were analyzed in duplicates serially diluted on 96-well flat-bottom microtiter plates (Greiner bio-one) coated with 1μg/ml NP_4-BSA or NP_{20}-BSA conjugates (Biosearch Technologies) in 50μl/well coating

buffer (15mM Na_2CO_3, 35mM $NaHCO_3$) overnight at 4°C. For anti double-stranded DNA ELISA, plates were coated with Poly-L-Lysin (10 μg/ml) in 10mM Tris/ 0.1mM EDTA / pH8.0 overnight at 4°C, washed 3 times with Tris/EDTA buffer and coated with dsDNA (10 μg/ml) from calf thymus (Sigma) in Tris/EDTA. Plates were washed 3x with PBS, 0.05% Tween20 and blocked for 1h at room temperature with 275μl/well of PBS, 2%FCS. Binding of Abs from pre-diluted serum samples was allowed for 1h at room temperature. Captured NP-specific Abs were detected with goat anti-mouse IgM and IgG specific horseradish peroxidase (HRP)- coupled Abs (1:1000, Southern Biotech) and the ELISA was developed using o-phenoldiamindihydrochloride (OPD) substrate (20mM Na_2HPO_4, 7mM citric acid, 0.001% OPD, 0.035% H_2O_2) and acid stop (0.5M H_2SO_4). Optical density (oD) was measured at 490nm on a SpectraMax 190 Microplate Reader (Molecular Devices). Plates were normalized using ELISA IgM and IgG standards as internal reference.

Purification of murine B lymphocytes from spleen

B cells were enriched from splenic cell suspensions using the EasySep Mouse B cell isolation negative selection kit (EasySep #19854, StemCell Technologies, Inc.) according to the manufacturer's instructions. In short, spleen cells were resuspended in MACS buffer (PBS, 2% FCS, 2mM EDTA), surface blocked with rat serum and immunomagnetically enriched for untouched naive B cells. Purity of isolated B cells was verified by surface stain for CD19. Usually, an enrichment of > 95% was achieved.

In vitro cultivation of primary murine B cells

Splenic B cells were cultured with a starting concentration of $1x10^6$ cells/ ml in R10 medium (RPMI1640, 10% fetal calf serum (FCS), 2mM glutamate, 1mM sodium pyruvate, 50 U/ml penicillin G, 50 μg/ml streptomycin, 50 μM β-mercaptoethanol) for 48h at 37°C and 5% CO_2, supplemented with 10μg/ml anti-IgM $F(ab')_2$ Ab (AffiniPure $F(ab')_2$ fragment goat anti-mouse IgM, μ chain specific, Jackson ImmunoResearch), 10μg/ml rat anti-CD40 Ab (clone FGK45, (Rolink et al., 1996) and 0.1U/ml IL-4 (mouse IL-4, premium-grade, Miltenyi Biotec).

In vitro migration assay of activated B cells

Migration assays were performed as described in Liu et al. (2016). ICAM1-Fc fusion protein was obtained by cloning a PCR fragment (fwd primer: tgtcacgaattcgcaggtatccatccatcccagagaag, rev: atgcagatctgttattttgagagtggtacagt) obtained using murine lung cDNA as a template. The PCR product was cloned into pFUSE-rIgG-Fc2 (Invivogen) via BglII/EcoRI restriction sites, replacing the endogenous signal peptide with the vector encoded IL-2 signal sequence and the membrane domain with a rabbit IgG Fc2 part. ICAM-1Fc was purified from the supernatant of transfected 293 cells by Protein A Sepharose (Thermo Sientific). 8-well polymer chambered coverslips (Ibidi) were coated with 10μg/ml Protein A (Sigma Aldrich) and 5μg/ml recombinant mouse CXCL13 or CXCL12 (carrier-free, Biolegend) in 200μl PBS/well for 2h at room temperature. Chambers were rinsed once with 10mg/ml fatty acid-free BSA (Sigma Aldrich) in PBS and coated with 10μg/ml ICAM-1 Fc in PBS for 2h at room temperature. After additional washing chambers were blocked with 10mg/ml fatty acid free BSA in PBS over night at 4°C. The coverslips were finally washed with pre-warmed migration medium (phenol red-free RPMI1640, 2mM glutamate, 1mM sodium pyruvate, 50 U/ml penicillin G, 50 μg/ml streptomycin, 50 μM β-mercaptoethanol, 10mg/ml fatty acid-free BSA) and kept humidified at 37°C until use. B cells were washed by centrifugation at 300xg for 5min at 4°C and seeded in pre-warmed phenol red-free migration medium at a concentration of $5x10^5$ cells/ ml in 200μl/well. F-Actin of living cells was labeled using SiR-actin (1:1000, Spirochrome).

Spinning disc confocal microscopy

Live cell migration was analyzed using the Zeiss Spinning Disc Axio Observer Z1, with a LD LCI Plan-Apochromat 25x/0.8 Imm Korr DIC M27 or Plan-Apochromat 63x/1.40 Oil M27 objective. All experiments were performed at 37°C and 5%CO_2. Time series were acquired using an Evolve camera and Zeiss Zen software. Fluorescence (638nm laser wavelength) and DIC was recorded. Images were processed with the Fiji software using manual tracking macro to track cell migration. The freeware Chemotaxis and Migration Tool (Ibidi) was used for further quantification of cell velocity.

Adoptive B cell transfer

Immunization of donor (WT and EFhd2KO) and recipient mice with SRBC and the isolation of splenic B cells from the donors at d7 post antigen challenge was performed as described above. $20x10^6$ B cells per genotype were fluorescently labeled with Hoechst and CMTPX (both Thermo Scientific) or vice versa. WT and EFhd2KO B cells were mixed in a 1:1 ratio and transferred i.v. into recipient mice. 24h post transfer and 4h before imaging, follicular dendritic cells (FDCs) of recipient mice were *in vivo* labeled via i.v. application of anti-CD21/35-Atto590 F(ab')-Ab or CD21/35-Alexa647 F(ab')-Ab (coupled in-house at DRFZ, Berlin). For multi-photon microscopy of B cells in splenic germinal centers, spleen was isolated, transferred into pre-warmed R10 medium and cut into slices (1-2mm thickness). Migration of cells was tracked for 30-50min. B-T-conjugates were quantified as described previously (Lee et al., 2017; Reinhardt et al., 2009). Briefly, $15x10^6$ splenic B cells from WT and EFhd2KO mice, isolated as described above, were transferred i.v. in a total volume of 75μl PBS into congenically marked Ly5.1 recipient mice. Recipients were challenged with 100μg NP-KLH in alum (described above) 24h later and analyzed at d14 and d21 post antigen application.

Imaging Cytometry

Samples were prepared as described above (Detection of surface antigens by flow cytometry) and subjected to analysis with an Amnis® FlowSight (Luminex Corp., Austin, TX). Fluorescence spillover was compensated using single-stained cells. Samples were focused based on the signal of CD45.1 (Channel06, PE/Cy7). Debris was gated out from the focused cells based on area and aspect ratio of the bright field (BF). For each sample 3000 events in the $CD19^{+}/CD4^{+}$ double positive gate were recorded. Data were analyzed with IDEAS v6.2 (Luminex Corp.).

In silico GC model

In silico germinal center modeling was as previously described (LEDA model) (Meyer-Hermann, 2014; Meyer-Hermann et al., 2012; Meyer-Hermann et al., 2018). The motility properties were introduced in Figge et al. (2008) and fine-tuned in Binder and Meyer-Hermann (2016). The multiple B-T-interactions have been introduced in detail in Meyer-Hermann et al. (2018).

QUANTIFICATION AND STATISTICAL ANALYSIS

Values were assessed for Gaussian distribution using the Shapiro-Wilk normality test. Mann-Whitney test was used for non-Gaussian distributed datasets. Datasets revealing Gaussian-like distribution were assessed by Student's t test. Differences between the analyzed groups were considered to be statistically significant with p values < 0.05. Data were analyzed using Prism (GraphPad).